ATMOSPHERIC SODIUM MEASUREMENTS AT 23° SOUTH

by

Volker W. J. H. Kirchhoff

Adviser

B. R. Clemesha

Relatório LAFE-197

June 1972

Submitted in partial fulfillment of
the requirements for the degree of
Master of Science

PR — Conselho Nacional de Pesquisas (CNPq)
Instituto de Pesquisas Espaciais (INPE)
São José dos Campos — SP — Brasil

ATMOSPHERIC SODIUM MEASUREMENTS AT 23° SOUTH

by

VOLKER W. J. H. KIRCHHOFF

Adviser

B. R. CLEMESHA

RELATÓRIO LAFE-197

JUNE 1972

SUBMITTED IN PARTIAL FULFILLMENT OF
THE REQUIREMENTS FOR THE DEGREE OF
MASTER OF SCIENCE

PR - Conselho Nacional de Pesquisas
Instituto de Pesquisas Espaciais
São José dos Campos - SP - Brasil

PRESIDÊNCIA DA REPÚBLICA
CONSELHO NACIONAL DE PESQUISAS
INSTITUTO DE PESQUISAS ESPACIAIS
São José dos Campos - Estado de S. Paulo - Brasil

ATMOSPHERIC SODIUM MEASUREMENTS AT 23° SOUTH

by

VOLKER W. J. H. KIRCHHOFF

This report contains elements of INPE's research program and its publication has been approved by

Fernando de Mendonça
Fernando de Mendonça
General Director

PREFACE

The Institute of Space Research (INPE) offers to graduates the possibility of working towards a Master of Science degree in the field of Space Science.

Graduate progress is measured on a credit basis. One credit unit corresponds to a minimum of sixteen class-hours, or 64 hours of research work. At least 36 credits are necessary for the Master's degree, 12 of them being attributed to a thesis. The minimum grade is B.

The author attended 8 courses: Applied Mathematics, Probability Theory, Modern Physics, Classical Mechanics, Physics of the Upper Atmosphere, Electrodynamics, Quantum Mechanics, and Laser Theory and Applications.

The courses were ministered on a three hour per week basis and the thesis research lasted for about a year.

The present work is thus the complement for the requirements of the Master's degree.

ABSTRACT

This report describes the technique of measuring atmospheric sodium densities. Chapter I deals with the general phenomena of sodium glow and the description of the basic equipment used for the measurements. Using the laser radar facilities of INPE's MIRO II Project, the main task was to adapt the equipment for the measurements of atmospheric sodium. A dye laser was constructed, with three temperature controlled Fabry Perots acting as band narrowing and tuning elements. Atmospheric sodium profiles were also deduced by the twilight glow method. The twilight measurements and some resulting profiles are shown in Chapter II. In Chapter III we show the laser measurement theory with the tuning arrangements and some interesting observations of the performance of the dye laser itself. The results of the radar measurements and the analysis of the data are also presented in Chapter III.

CONTENTS

LIST OF FIGURES

LIST OF TABLES

CHAPTER I

INTRODUCTION

1.1 - THE AIRGLOW AND THE SODIUM D LINES

The word *airglow* designates the radiation emitted by the earth's upper atmosphere (except radiation due to aurorae).

Though the first discussions about aurora were a long time ago, (Anaximenes, Anaxagoras, Aristotle, around 500 BC) studies of the airglow began only around 1900, when the light of the night sky was understood as the radiation flux of a great number of stars too faint to be seen individually. Only in 1933, *Dufay* showed that at least in part the light must come from the self luminescence of the atmosphere.

Twilight glow is the airglow emission at a time when sunlight is shining on the emitting region of the atmosphere from below.

Significant observations may be made during twilight glow. Measurements of the intensity of the twilight emission throughout twilight and into the night provide data which conveniently analyzed give information about height of emission, excitation process, abundance and vertical distribution (i.e., densities as a function of height) of the emitting substance.

It is easy to deduce a relationship between intensity and the emitting number of atoms of a substance if we assume simplifying conditions.

During the twilight periods certain spectral lines are emitted more strongly. Among others 5893 Å discovered in 1938. The sodium doublet (D_1 at 5896 and D_2 at 5890 Å) is the result of resonance scattering of sunlight. Several facts point to this excitation mechanism. For example, the theory of resonance scattering makes possible independent determinations of the abundance from the total D_1+D_2 intensity and from the D_2/D_1 ratio, and the estimates of abundance agree very well. Through the optical scattering excitation process the line width should be narrow, indicative of the doppler broadening for the temperature of the layer, but if ultraviolet light were the exciting agent the D lines would result from photodissociation of a sodium compound and the lines should appear wider. Furthermore a small degree of polarization was measured in the D lines as expected for resonance scattering.

The atomic transitions and the splitting of the energy levels in hyperfine structure are shown in figure 1.

In the radiative transfer theory the D lines may be treated as though they arise from resonance transitions, are scattered isotropically and are unpolarized.

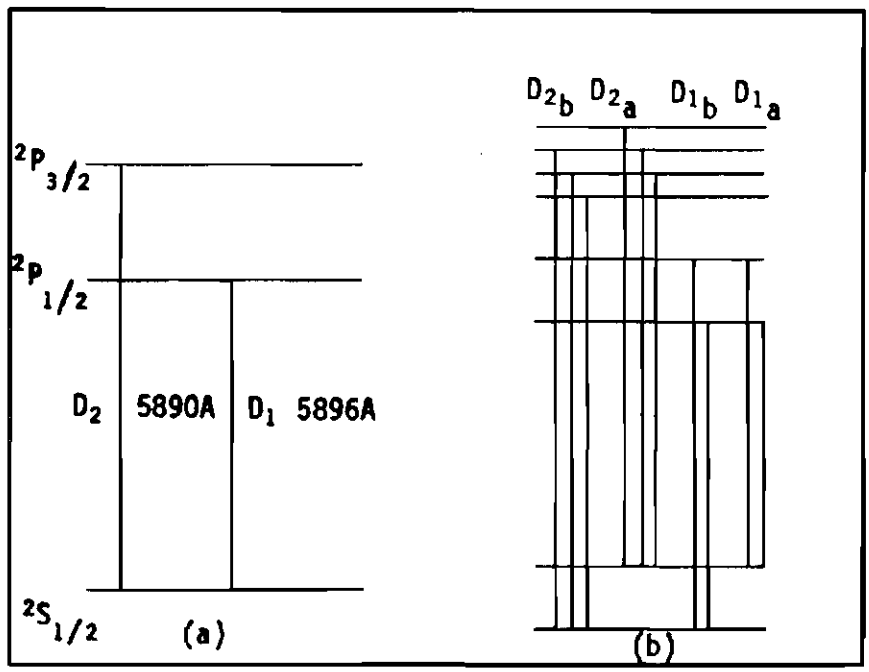

Fig. 1 - a) Energy levels of the sodium D lines

b) Hyperfine structure

None of these conditions is strictly true for D_2 and even D_1 is not actually a resonance transition when hyperfine structure is considered. Even though, a relation between the emission intensities and the density of sodium atoms is established; corrections are then superimposed to account for the theoretical approximations.

Let us now assume a simple two energy level system. The lower level is designated by 1 and the upper by 2. If there are N atoms per unit volume, an exciting beam of specific intensity I (watts x secs x cm^{-2}) raises $N B_{12} I_\nu$ atoms per second to level 2, B_{12} being the Einstein coefficient for intensities of isotropic radiation. These excited atoms are capable of emitting energy of frequency ν and thus the emitted energy per second per sterradian per unit volume is $N B_{12} I_\nu h \nu/4\pi$, where h is Planck's constant.

In the twilight studies the scattered signal is written in a different way because we can relate A_{21}, the spontaneous transition probability, to B_{12} and A_{21} in turn is related to the integrated absorption coefficient by the Füchtbauer-Ladenburg formula (see Appendix II). Thus, denoting the scattered intensity by I we have

$$I = N B_{12} I_\nu h \nu/4\pi = \frac{N A_{21} c^2 g_2}{8 \pi h \nu^3 g_1} I_\nu h \nu$$

$$= \frac{\lambda^2 g_2}{8 \pi g_1} N A_{21} I_\nu$$

where g_1 and g_2 are the multiplicities of the energy levels, c is the velocity of light, and λ the wavelength, or introducing the oscillator strength f value given by

$$f = \frac{m\, c\, \lambda^2\, A_{21}}{8\, \pi^2\, e^2}\ \frac{g_2}{g_1}$$

$$I = I_\nu\, N\, \frac{\pi\, e^2}{m\, c}\, f \qquad [\text{watts} \times \text{cm}^{-3} \times \text{sterad}^{-1}]$$

where e is the charge on the electron and m its mass. If we now interpret N as being the number of atoms per square centimeter column and measure I in units of 10^6 photons/sec/cm^2 /sterad then $4\,\pi\,I$ is in Rayleighs. For the sodium atoms, this simplified theory then shows a linear relation between I and N which is,

$$4\,\pi\,I = g\,N$$

where g is a constant.

Actually the source of atoms is concentrated in a layer, which to a first approximation may be considered as plane and parallel and the intensity will thus depend on θ, the angle between the normal to the layer and the direction of observation.

Thus

$$\cos\theta \; 4\pi I = g N$$

Taking into account that the incident sunlight must traverse the sodium layer on the day side, the previous linear relation must be modified by the self absorption function, approximated by an exponential.

Thus

$$4\pi I = AN \exp(-BN) \qquad (1)$$

where BN is the optical depth traversed by the incoming light. Adjustments are then made to fit the constants to the multiple scattering calculations and we get (see *Hunten*, 1967).

$$A = 7.65 \times 10^{-7} \; R \; cm^2$$

$$B = 4.15 \times 10^{-11} \; cm^2$$

$$N = \; atoms/cm^2$$

However, if the daytime abundance is greater than the twilight one, the results must be modified. The absorption in the exponential is 2/3 on the day side and 1/3 on the twilight side, to a first approximation, according to *Rundle et al*, 1960. Thus, an extention

of (1) gives

$$4 \pi I = A N_t \exp \left[-B(N_t + 2N_d)/3\right]$$

or

$$4 \pi I = A N_t \exp \left[-B N_t(1 + 2R)/3\right]$$

where N_t and N_d are respectively the abundances in the twilight and in the daytime and $R = N_d/N_t$. Thus the twilight abundances may be found knowing the daytime abundance or by approximating with R = 1. Alternatively it is possible to measure the factor R by treating the two D lines separately, and calculating the D_2/D_1 ratio. The effective absorption cross section differs by a factor of 2 but at zero optical depth the intensity ratio is 1.79 because the two Fraunhofer lines have different depth.

$$D_2/D_1 = A_2/A_1 \exp \left[-N(B_2-B_1)(1 + 2R)/3\right]$$

$$D_2/D_1 = 1.79 \exp \left[-2NB(1 + 2R)/9\right]$$

Thus we established a second equation for the calculation of the two unknowns R and N and so the combination of ratio and intensity measurements makes it possible to find R without having to observe the dayglow.

1.2 - THE ORIGIN OF THE SODIUM IN THE ATMOSPHERE

Once the sodium emission was discovered, many theories appeared to explain its origin in the atmosphere.

Though the twilight sodium measurements only infer abundances of the neutral atomic fraction, it is possible and likely that the ionized and chemically bound fractions are quite large. A dayglow enhancement of the sodium content in the atomic form seems to confirm the presence of a considerable reservoir of molecular sodium which becomes dissociated during the day.

The sodium present in the atmosphere may be of *terrestrial* or *extraterrestrial* origin. The principal terrestrial sources are sea salt, volcanic and continental dust, and possibly debris from thermo nuclear bomb tests.

From extraterrestrial sources, the sodium may be introduced by meteors, interplanetary dust, interstellar dust, and ejections from the sun.

The characteristics of the sodium layer are its altitude, the neutral atomic state of the atoms and their concentration, and whatever the source is, it must satisfy these conditions.

According to a study of *Junge, Oldernberg and Wasson* (1962), the possible transport of sea salt to high altitudes is not sufficient to explain the observed sodium concentrations except under certain favorable assumptions. There is a lack of means to produce atomic sodium salt particles. A continental origin is subject to the same objections and a volcaninc origin may be excluded because the sodium abundances remain fairly constant from year to year. From *Hunten*'s data it is possible to see that the amount of bomb debris from the Castle test series (1954) injected into the atmosphere was considerably less than that already present due to the natural sources.

From calculations of annual influxes, the same authors concluded that the solar corpuscles contribute only a minor fraction of the sodium influx, and that meteors provide the most satisfactory origin of the sodium because they evaporate at the correct altitude.

About the same subject *Hunten and Wasson* (1967) wrote that a salt particles source can not be entirely dismissed because there is a violent vertical mixing in the high atmosphere during the polar night and this might be able to carry the salt particles upward more efficiently than any of the processes considered by *Junge et al.* However the same vertical mixing would also stir up any dust of interplanetary origin that had fallen below the 90 km region. One is therefore still left with the conclusion that the interplanetary origin is intrinsically more probable but with no direct evidence.

More recently, *Gadsden* (1968), analyzes a source of dust particles from which sodium atoms are released by the action of sunlight (this kind of source was postulated as a result of rocket measurements) and the meteoric origin. He concludes that sufficient data do not exist to decide between the dust and the meteoric ablation hypothesis and indicates that a very fruitful line of enquiry is to obtain a 24 hr. picture of the density of atomic sodium as a function of height. He finishes with the observation that the absence of data on the abundance of atomic sodium during the night is notable and we feel that with this connection our work may reach some importance.

1.3 - ROCKET MEASUREMENTS IN THE DAYTIME

Assuming that the sodium layer is present in the daytime, *Donahue* (1956) and *Brandt and Chamberlain* (1958) predicted the corresponding dayglow intensity. Earth albedo as well as attenuation of the incident light by the sodium layer itself in twilight were taken into account.

Ground based observations of the dayglow by means of a Zeeman photometer were first performed by *Blamont and Donahue* (1961, 1964) followed since then by a number of workers.

The first results showed an enhanced sodium dayglow. To verify or disprove this enhancement, rocket flights were performed (*Hunten and Wallace*, (1967), *Donahue and Meier*, (1967)).

The results were compared with calculations based on a model of resonance scattering of sunlight by the sodium atoms and showed the existence of a sodium layer containing 16×10^9 atoms/cm^2 centered at 92.4 km. These atoms were found to be concentrated in a very thin layer of about 5 km. The twilight glow a few hours before gave 6.2×10^9 atoms/cm^2 in a layer 8.8 km wide at 89.8 km. These data showed also conclusively that the scale height of the sodium distribution can be as small as 2 to 3 km, or approximately one half that of the atmosphere on the topside. If the atomic sodium is supposed to be in quasi photochemical equilibrium, it follows that the topside of the sodium distribution will show a scale height similar to, if not precisely identical with that of the atmosphere in general. Therefore the rocket data became important because they provide a strong inconsistency with the basic assumption of photochemical models and the postulation of a source of dust particles (from which sodium atoms are released through the action of sunlight) arose.

1.4 - VARIATIONS OF SODIUM DENSITIES

In general, the day to day variations of sodium abundances are quite large (around a factor of 2) but the ratio of abundances found in the morning to that found in the evening are very nearly equal to one for twilight measurements.

Because of this variability and also because of weather conditions it is necessary to accumulate several years of data at any

station before the typical behavior can be deduced. Saskatoon and Haute Provence are the only two stations which satisfy the condition above but some information is available at a number of other stations (see *Hunten*, (1967)).

A seasonal variation does exist. In the Northern Hemisphere where most of the observations are made there is a pronounced maximum of sodium abundance during the winter and a minimum during summer. It is interesting to note that the same seasonal variation occur in the Southern Hemisphere as was reported by *Tinsley and Jones* (1962) who based their conclusion on measurements made in New Zealand, and confirmed by *Jones* (1963), *Hunten et al* (1964) and *Gadsden* (1964). However, measurements made at Tamanrasset (23^{o} N) suggest that this enhancement may not be present at latitudes lower than, say, 45^{o}.

Night observations were started in early 1969 by *Bowman et al* (1969) at Slough, England, by means of a narrow band dye laser radar. (This technique is now introduced at São José dos Campos, a South latitude station. The equipment and measurements are described in Chapter III).

Since then measurements have been made with the following conclusions (*Sandford and Gibson*, (1970), and *Gibson and Sandford*, (1971)).

The seasonal variation of the abundance at night was found to be similar to that observed by the twilight method with the scatter in the night time values being less than that of the corresponding twilight values.

An unnusual layer at 103 km was observed on two nights, during a year's observations.

The winter maximum of abundance seems to be a result of the appearance of sodium on the lower side of the layer and the summer minimum caused by a loss of sodium from the topside. The topside scale height at an altitude of 102 km is less than 2 km. The results of our own measurements are discussed in Chapter III.

1.5 - SPECTROSCOPIC REMARKS ON THE SODIUM DOUBLET

From quantum mechanics it is well known that a given atom may only assume a certain number of definite stationary energy states defined by the quantum numbers.

The normal state of the sodium atom is the $3\ ^2S_{1/2}$ state. Here the number 3 stands for the principal quantum number n, the number 2 for the multiplicity of the energy level, S is the spectroscopic notation to designate that the angular momentum $\ell = 0$ and 1/2 is the value of the total angular momentum J = L + S. All energy states are actually double (with the exception of the S state). This is because if one assumed that the resultant spin for all the electrons forming the atom core is zero, i.e., that the spins of the electrons in the core neutralize each other in pairs, there remains only the spin of the valency electron, because

the sodium atom has 11 electrons in the sequence $1s^2\ 2s^2\ 2p^6\ 3s$. Thus the spin angular momentum s may be $+1/2$ or $-1/2$ and for each value of l two values for J arise, so that the multiplicity is 2.

The first excited energy level is for $n = 3$, $l = 1$ so that $J = 1+1/2 = 3/2$ and $J = 1-1/2 = 1/2$ and the notation is thus $3\ ^2P_{1/2}$ and $3\ ^2P_{3/2}$.

When a continuous spectrum of light of wavelength from 2000 to 6000 $\mathring{A}$ is sent through sodium vapour, it is found that only the lines of the principal series $3\ ^2S_{1/2} - 3\ ^2P_{1/2}$ (5896 $\mathring{A}$) and $3\ ^2S_{1/2} - 3\ ^2P_{3/2}$ (5890 $\mathring{A}$) are absorbed since at ordinary temperature all sodium atoms are in the ground state and only the two states above may be excited. With the return to the normal state emission of the D lines occurs. Thus a simplified energy level diagram would consist in the ground level and the two excited ^2P states.

With the introduction of apparatus of high resolving power, the D lines show their hyperfine structure, which can be accounted for by a nuclear spin $\frac{Ih}{2\pi}$ and a corresponding magnetic moment. The nucleus having a nuclear spin of quantum number I, the total angular momentum will be

$$J + I = F$$

F being the hyperfine quantum number. If $J \leq I$ as for sodium ($I = 3/2$) there are $2J + 1$ values of F so that we have a splitting of the $J = 3/2$ level in $2(3/2) + 1 = 4$ sub levels, with $F = 3, 2, 1$ and 0; for the $J = 1/2$ level, $2(1/2) + 1 = 2$ sub levels, with $F = 1$ and 2. The selection rules for the h.f.s are $\Delta F = 1$ or 0, but $F = 0 \rightarrow F = 0$ is forbidden. The result of the above considerations is shown in the energy level diagrams of figure 1.

1.6 - THE BASIC EQUIPMENT

The equipment used in the present work comprises the laser radar facilities of INPE's MIRO II project.

The laser radar technique was developed in the early 60s by a number of workers (*Fiocco and Grams* (1964), *Bain and Sandford* (1966) *Clemesha et al* (1966)), and since then has been used by a number of researchers throughout the world to obtain atmospheric density profiles and related properties.

As in an ordinary microwave radar, the system consists of a transmitter and a receiver. The heart of the receiver system is a photomultiplier tube (PMT) which has the advantages of low noise and high sensitivity at the wavelength of interest. Unwanted signals and wideband noise are removed by interference filters of the Fabry Perot

type. The signal to be detected is introduced into the PMT by a spherical fixed high quality mirror (M2) to which the signal is fed through a plane mirror (M1) which collects the light from above. The signal from the PMT is then processed and counted in a digital analyser and the counts are printed. This electronic equipment is rather complicated and was described by *Rodrigues* (1970).

A schematic lay-out of the laser radar is shown in figure 2.

For the twilight measurements, a Coherent Optic's model 410 A tunable etalon, with free spectral range 20 Å was used in front of the PMT.

In a laser radar, a laser is the transmitting source. It provides an intense beam of light of short duration, monochromatic and collimated, i.e., coherent. This light pulse passes through a rotating shutter to cut off the fluorescence radiation and to reduce the beam diameter sufficiently for it to pass through the 1 cm aperture of the shutter, it passes first through a convex lens, then through a system of lenses and mirrors that acts as a collimator, decreasing the angular beamwidth going finally to a plane mirror that acts simultaneously as a transmitter and receiver (see figure 2).

The system is used for investigations of the upper atmosphere, operating with a ruby laser, and through Rayleigh scattering by air molecules density profiles are deduced.

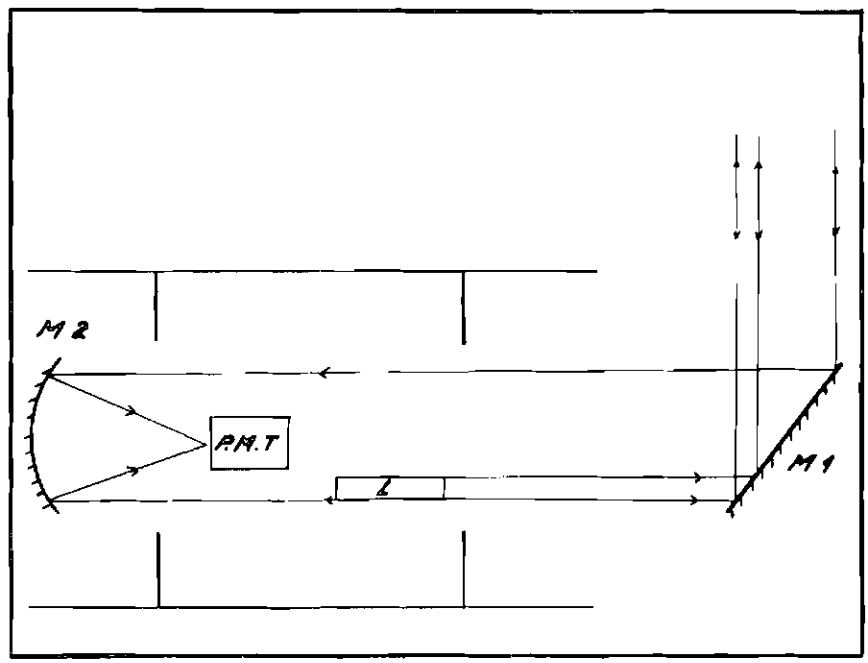

Fig. 2 - Schematic lidar lay out

For our purposes a dye laser will be used, as the radar transmitter. This instrument furnishes a pulse of energy of a few milijoules. Using Rhodamine 6G, in a solution of ethanol concentrated near 1.0×10^{-4} mol/l, the spectral extent is of the order of 150 Å, centered at the sodium D lines.

The table below shows the parameters of the optical radar.

TABLE I

THE LASER RADAR PARAMETERS

Energy per pulse	4 mJ
Wavelength	589.0 nm
Bandwidth	0.005 nm
Repetition rate	10 per min
Pulse duration	0.5 μs
Receiver efficiency	0.01
Height interval used	2 km
Receiving area	0.39 m^2

CHAPTER II

TWILIGHT MEASUREMENTS

2.1 - GEOMETRIC RELATIONS DURING TWILIGHT

In the case of zenith observations, the twilight scattering geometry is as shown in figure 3. We need a relation between time and actual shadow height, for the data reduction, and will derive it below.

The point where the sun rays are tangential to the earth's surface is called the terminator. The tangential rays cross the zenith direction at a point which defines the geometrical shadow height, Z_1. However this geometrical height is not the effective shadow height because of extinction or screening effects of the lower atmosphere. The extent of extinction or screening by the atmosphere on the incident light beam depends on the wavelength of this radiation.

The screening height h_o is defined as the height of an effective shadowing edge that would give a shadow equivalent to the real one. Z_2 is the true or screened shadow height.

Looking at figure 3, we calculate Z_2 using triangular relations

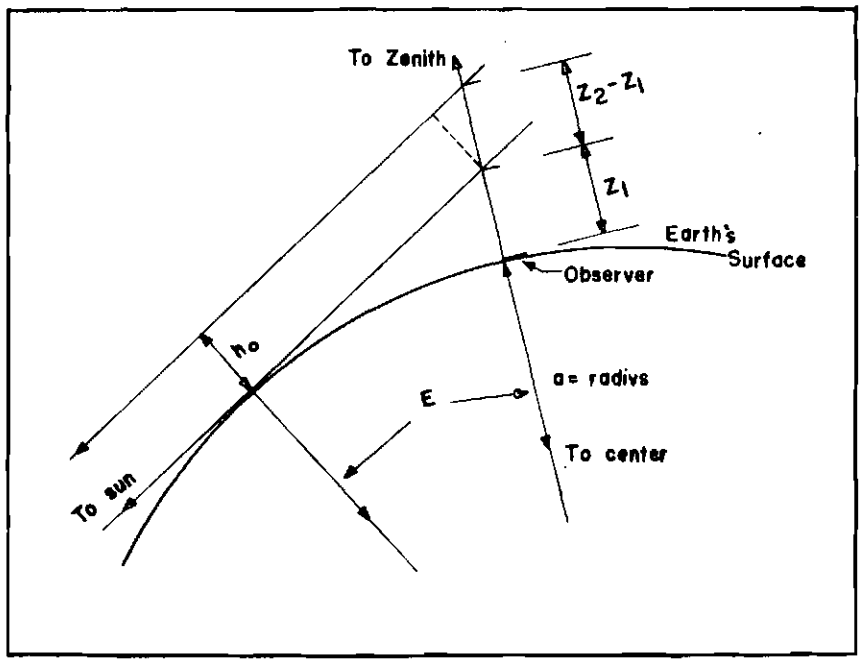

Fig. 3 - Simple twilight scattering geometry

$$a.\sec E = a + Z_1 \, , \; Z_1 = a \, (\sec E - 1)$$

and

$$Z_2 - Z_1 = h_o \sec E$$

Thus we have

$$Z_2 = (a + h_o) \sec E - a$$

where a is the earth's radius (6371 km) and E is the sun's elevation angle (or depression angle). We thus have a relation between the effective shadow height Z_2 and the sun's elevation angle E.

Let us turn now to figure 4, which illustrates the celestial sphere.

Applying the rules for spherical triangles we get for E,

$$\sin E = \cos\phi \cos L \cos D + \sin L \sin D$$

where ϕ is the local hour angle, L is local latitude and D is the sun's declination.

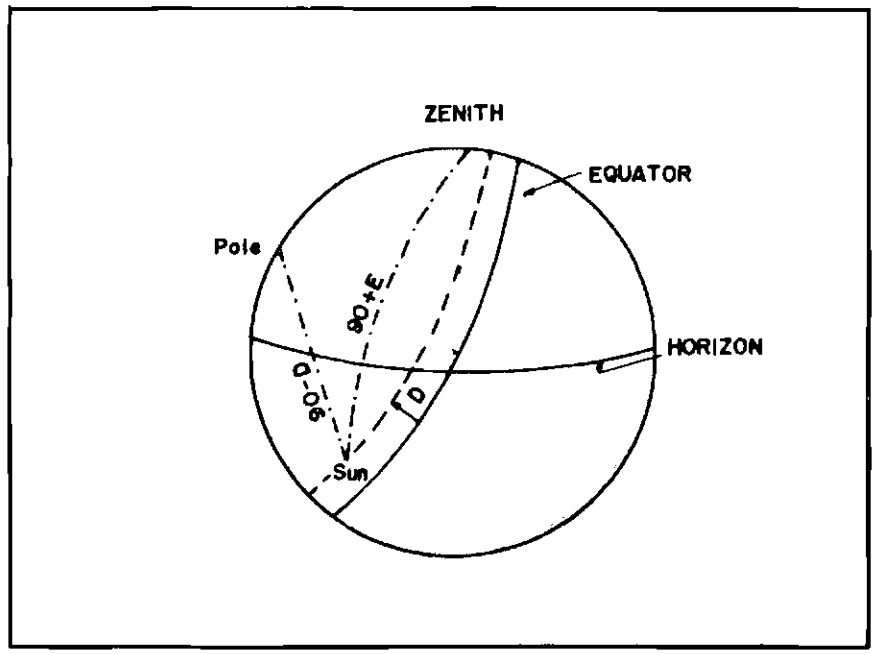

Fig. 4 - The sun-pole-zenith sphericle triangle

The local hour angle is simply related to the Greenwich hour angle (GHA) by

$$\phi = GHA - \lambda_W$$

where λ_W is longitude toward west.

For São José dos Campos we have $\lambda_W = 45.86^o$ and $L = -23.212^o$ so that by substitution with cosL = .9191, sin L = -.3942 we get

$$\sin E = \cos(GHA-45.86).9191 \cos D-.3942 \sin D$$

The final relation between GHA and Greenwich mean time (GMT) is given by

$$GHA = \frac{GMT \ \ (hrs) \ + \frac{min}{60}}{24} \ x \ 360 + \Theta$$

where Θ is the GHA for midnight on the day in question.

Data of sunset and sunrise time, declination D and Θ values are given in the Nautical Almanac, for a given day.

A program for the calculations is listed in Appendix V.

2.2 - RECORDING OF A TWILIGHT SODIUM PROFILE

In order to obtain the twilight sodium profile we used the receiving system of the laser radar, described earlier.

An interference filter preceeded by a Fabry Perot etalon with tuning facilities were fixed in front of the PMT. The etalon (Coherent Optic's Inc. Model 410 A) was used in the scanning mode and a single free spectral range of 17 $\mathring{A}$ was isolated by the interference filter.

A measurement can only be made under clear sky conditions. The optical path to the PMT is then opened and a twilight run may begin.

One run consists of a number of measurements, each lasting around 40 seconds. Measurements are made each minute.

The scanning Fabry Perot interferometer is coupled to the digital analyser in such a way that the signal corresponding to a given wavelength is stored in a given channel. Each measurement normally involves 100 sweeps of the free spectral range of the Fabry-Perot and thus the final count stored in each channel is the sum of 100 measurements at a given wavelength. At the end of each complete set of 100 sweeps the content of the digital analyser is printed out on paper tape.

This print-out is then a spectrum of the twilight emission over the pass band of the interference filter, centered at the sodium D lines.

As the measurements show, the sodium D lines emitted during a twilight can easily be separated from the background during approximately twenty minutes.

2.3 - DATA REDUCTION

As already said, each twilight measurement consists of a number of twilight spectrums centered at the sodium D lines. These spectrums are presented in the form of pulses per channel in the output of the digital system. In the measurements already made the time interval per channel was 267 msec. We are thus able to plot the signal intensity in pulses per second as a function of channel or wavelength. Of course, the total area under this curve is proportional to the signal intensity in both lines. The desired unit is the Rayleigh and the transformation of units is shown in Appendix I.

Beside the signal measurements, we also measure the dark current noise, the background noise and the signal area from a reference source of known brightness.

A typical recorded twilight spectrum centered at the sodium D lines is shown in figure 5.

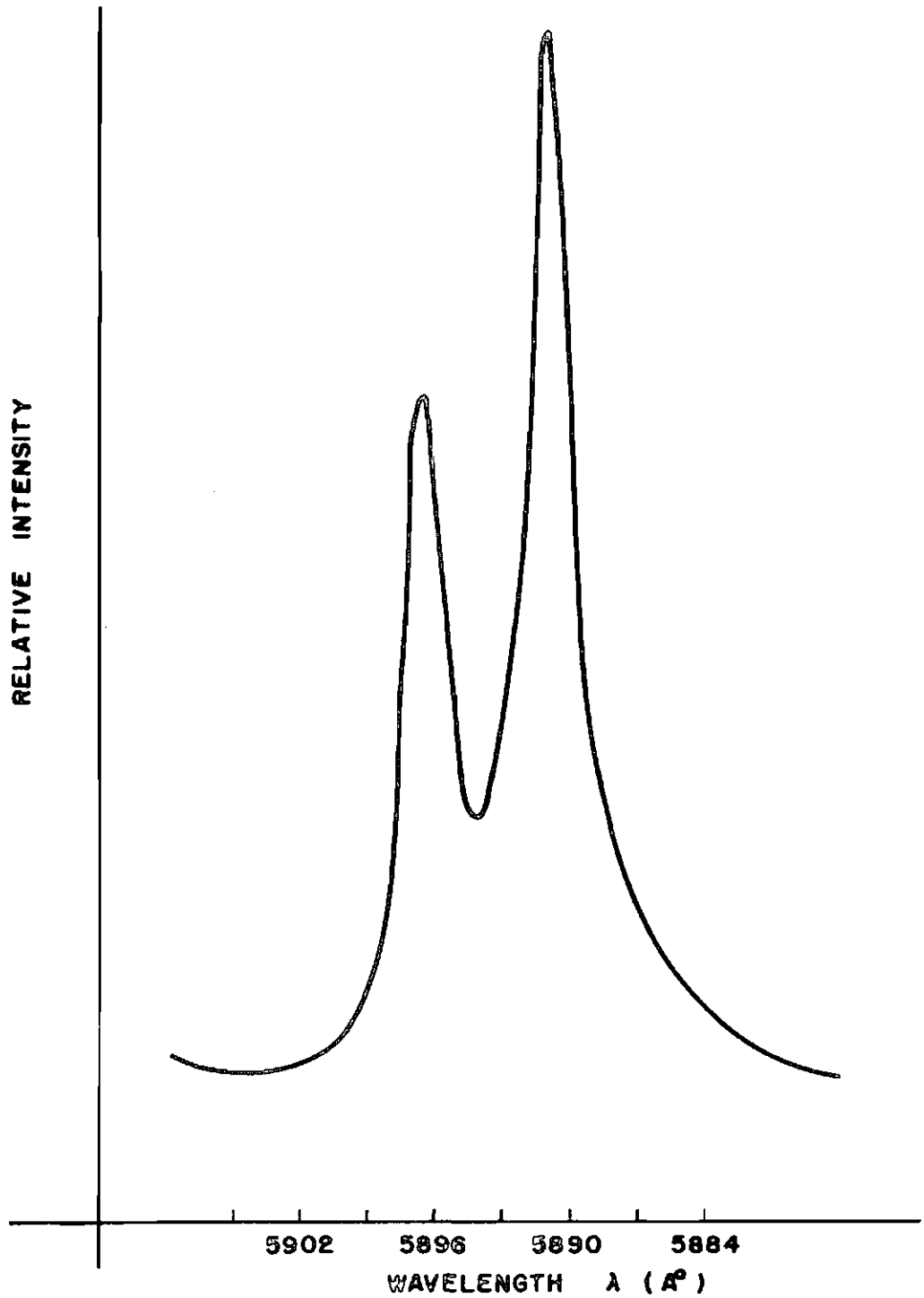

Fig. 5 - Typical twilight spectrum of the sodium D lines

With the areas converted in Rayleighs, we can plot signal intensities as a function of time. This is the first result from the data and can be used at least for comparisons. An example is figure 6.

It is possible to deduce the vertical distribution of the sodium atoms from the intensity versus time curve.

Because we have not a sharp edge at the shadow transition, the scattered signal I will be proportional to the convolution of the density n(z) and the shadow transmission function $T(z - z_1)$ where z denotes height above ground and z_1 the height at the transmission half peak value. Thus

$$I(z_1) \propto \int_0^\infty n(z)\, T(z - z_1)\, dz \qquad (1)$$

and this signal is a function of z_1. The integrand is zero at both limits, and in this case it is found that the operations of integration and differentiation can be exchanged, thus

$$\dot{I}(z_1) \propto \int_0^\infty n(z)\, \dot{T}(z - z_1)\, dz \qquad (2)$$

where $\dot{I}(z_1)$ and $\dot{T}(z - z_1)$ represent derivatives with respect to height.

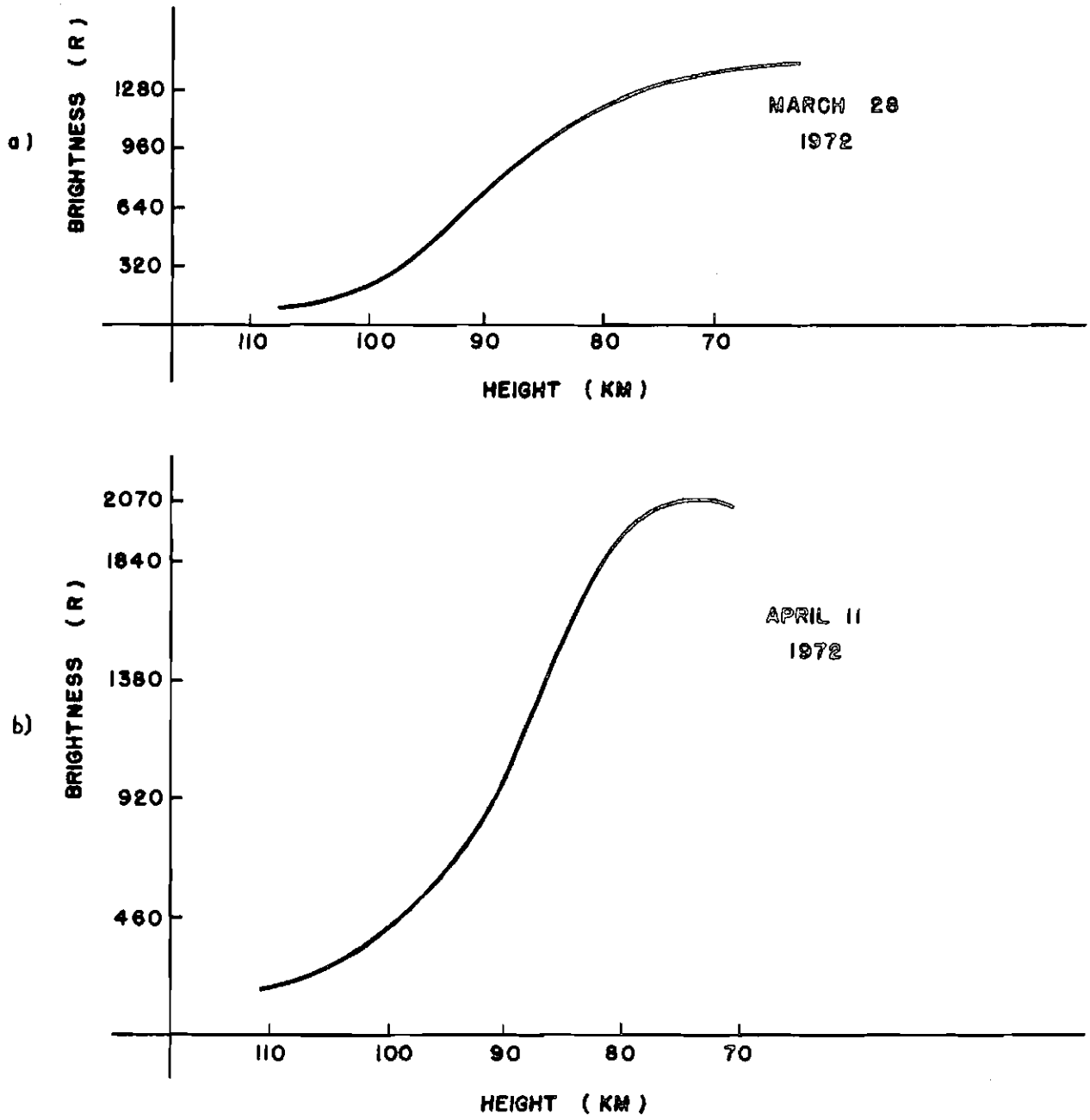

Fig. 6 - Twilight intensity variations

The method of deducing the vertical distribution n(z) is based on the relation above, that the derivative of the intensity is equal to the convolution of the number density of sodium atoms with the derivative of the transmission function. $\dot{I}(\dot{z}_1)$ is thus regarded as a smeared or broadened version of n(z) and the problem is to restore the actual shape of n(z) by a suitable process.

Mathematically if f(x) is a wanted function and g(x) is the approximation to it which is actually measured when observations are made with instruments of finite resolving power the relation between the two functions is

$$g(x) = \int h(x - x_1)\, f(x_1)\, dx_1 \qquad (3)$$

where h is the instrumental profile.

Applying the convolution theorem we get

$$G(s) = H(s)\, F(s) \qquad (4)$$

where G, H and F are respectively the Fourier transforms of g, h and f, or

$$F(s) = \frac{G(s)}{H(s)} = G(s)\ (H(s)^{-1} - 1) + G(s) \qquad (5)$$

It is found that the subsequent Fourier transform of the expansion of $H(s)^{-1} - 1$ as a polynomial in $\sin^n \pi as$ corresponds to the operation of taking finite differences over a specified interval a. In our case the instrumental profile is symmetrical and thus n is positive and even. Applying the Fourier transform to the last equation we have

$$f(x) = g(x) + C_n \qquad (6)$$

which means that the wanted function f(x) is equal to the observed function g(x) and a series of corrections C_n obtained by taking finite differences of g(x).

A first approximation is obtained with n = 2, and the correction term is the second order finite difference of g(x).

Bracewell discovered a graphical method to find C_2. It is quick and easy to use and the results are of useful accuracy when one does not aim at the highest precision. In the following we use his sharpening technique.

The transmission function is generally presented in terms of its screening height h_o and second moment σ^2. It takes into account

the extinction by Rayleigh scattering, absorption by ozone, extinction by haze and dust in the troposphere, refraction and the sun's finite size. For the sodium the parameters are h_o = 30.6 km and 2σ = 20.8 km, (*Hunten*, 1967).

We thus take the derivative from the previous figure, with the time scale replaced by the shadow height calculated in another section.

The restoring process is then to span a chord of vertical projection equal to 2σ. From the centre of the chord we trace a perpendicular to the axis and over the perpendicular we measure a distance 2L equal to twice the measure from the centre of the chord to the curve. We get point A, the first point of the restored vertical profile. The construction is shown in figure 7. The whole curve is constructed by finding the other points obtained by the above procedure.

The convertion from R/km to the sodium density scale is the next step. Conversion tables have been prepared in the form of intensity curves (in Rayleighs) versus total sodium abundances (in atoms/cm^2) and with the derivations above the R/km axis is transformed into a density scale. Resonance extinction by the sodium itself and multiple scattering is taken into account. Details and references are given by *Hunten* (1967).

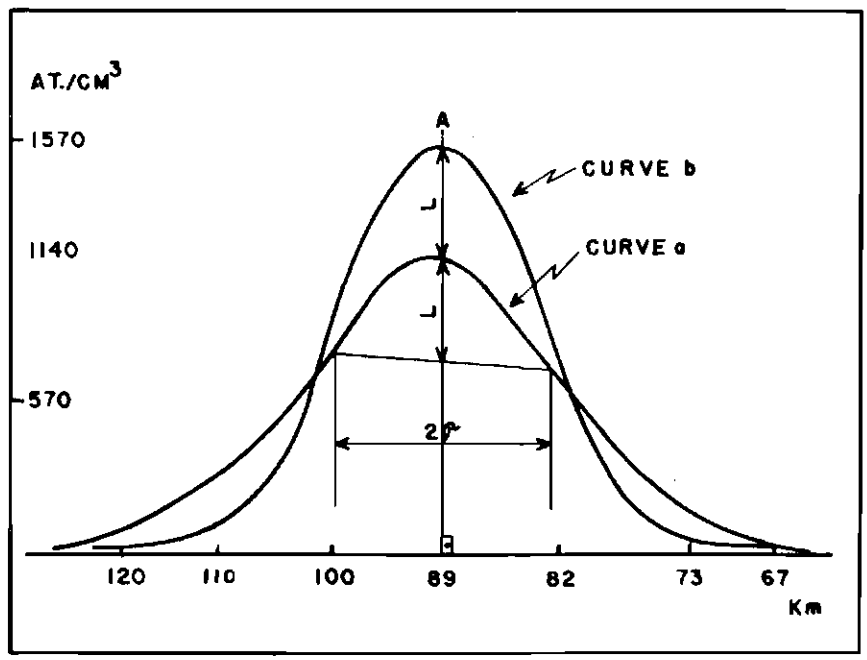

Fig. 7 - Bracewell's process

a) signal derivative

b) restored density profile

It must be noted that for the twilight data up to March, 1971, we were not able to measure the background light level very accurately and therefore the sodium abundances were calculated with an error estimated to be of the order of ±10 to 20%.

2.4 - RESULTS

As final results for the twilight measurements we show the data presented in figures 8 and 9, and 27. As there is some evidence of a cometary origin for the sodium in the atmosphere, the passage of the earth through the plane of the orbit of comet Encke on February 23, 1971, could be supposed to enhance the sodium signal to some extent. Unfortunately it was not possible to get a great number of twilight sodium profiles before or after the comet's passage because of instrumental problems and also poor weather conditions. Anyway, due to the comet or not, the sodium abundance measured on February 24, 1971, was the highest.

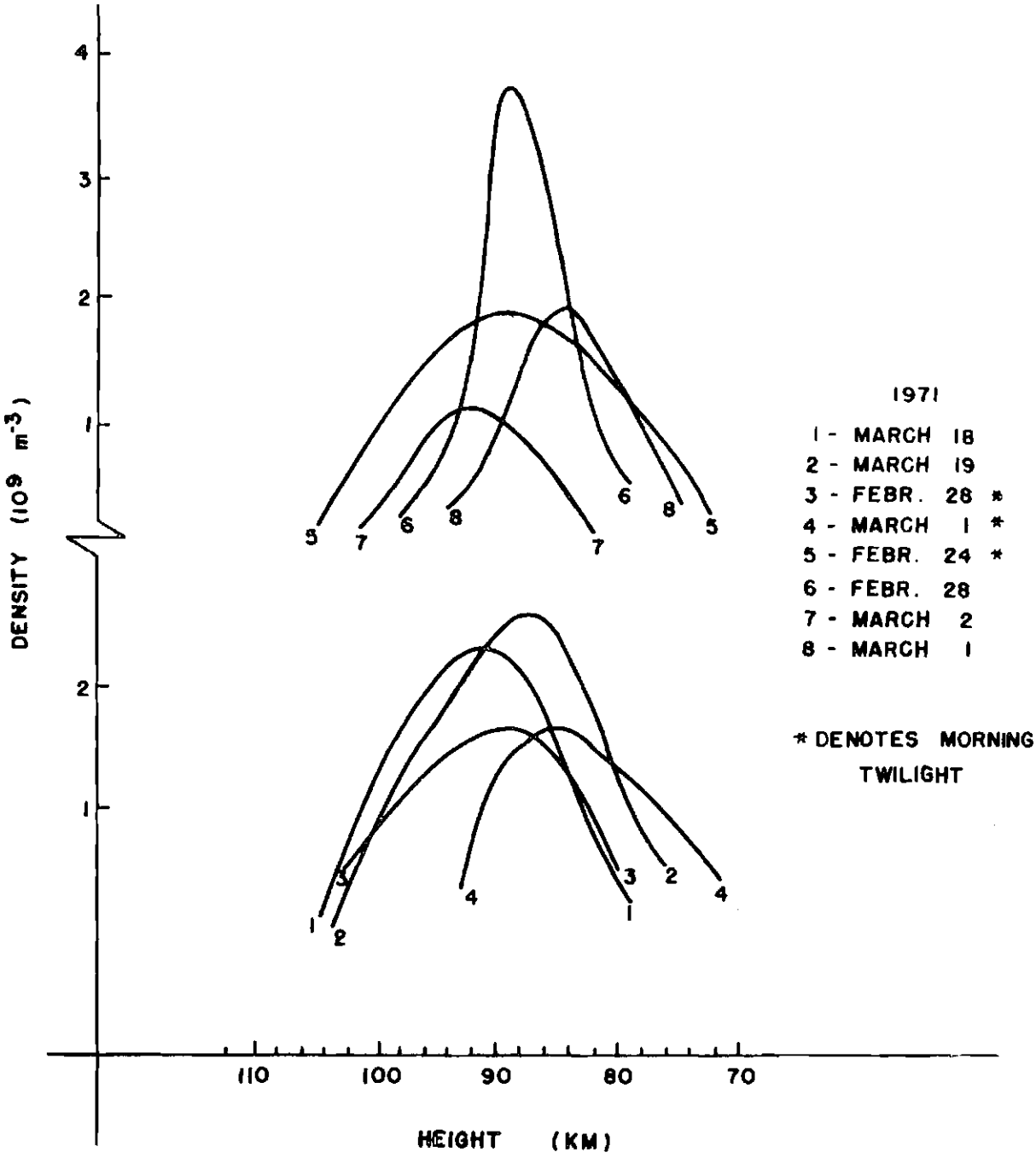

Fig. 8 - Atmospheric sodium density profiles measured in the twilight periods

DATE 1971 MONTH DAY	ABUNDANCE ATOMS m^{-2} X 10^{13}	HEIGHT OF PEAK KM	MAXIMUM DENSITY X 10^{9} m^{-3}
2 *24	5.30	90	1.90
2 *28	4.00	89	1.70
2 28	3.60	89	3.84
3 *01	3.50	86	1.70
3 01	2.28	84	1.93
3 02	1.73	93	1.10
3 18	3.10	92	2.30
3 19	1.90	89	2.60

* denotes morning twilight

Fig. 9 - Some twilight results for 1971

CHAPTER III

LASER MEASUREMENTS

3.1 - THE LASER RANGE EQUATION

Resonance radiation is absorbed and re-emitted very rapidly so that the process can be regarded as a scattering one; the process is called resonance scattering.

A parallel beam of light of intensity I_0 traversing a layer of atoms is decreased by scattering or by absorption and scattering. We thus write

$$I'_\nu = I_0 (\nu) e^{-C_\nu nx}$$

Here I'_ν is the intensity at x, n is the number of atoms per unit volume and C_ν is the extinction cross section, where

$$C_{ext}(\nu) = C_{abs}(\nu) + C_{sca}(\nu)$$

The cross sections are measured in units of area. We have also $C_{abs}(\nu) = k_\nu/n$, where k_ν is the absorption coefficient, measured in inverse length units.

In our case, a beam of light will be transmitted vertically through the atmosphere up to a height h and scattered by a volume V. At the ground, the beam has a power P_o, the light pulse a duration of t_o seconds and N_o photons at $\lambda 5890$ Å are transmitted. Up to height h the beam is attenuated by the atmosphere. The number of photons remaining at height h is $N_o T$ where T is the transmission coefficient for the atmosphere at the specified wavelength.

The laser pulse has a finite length $L = ct_o$, where c is the velocity of light. Hence at instant t_1, the front of the pulse reaches the receiver, scattered from height h, and at instant t_2 the end of the pulse reaches the receiver but now the front of the pulse is scattered from height h + dh. So we have

$$ct_1 = 2h$$

and

$$ct_2 = 2(h + dh)$$

Since $t_2 - t_1 = t_o$,

$$dh = ct_o/2 \qquad (1)$$

We will now assume that the absorption of resonance radiation is not saturated, that the emission takes place isotropically with unity quantum efficiency and negligible delay (of the order of

16 ns or a range of 5m).

We have at height h, where the beam is incident on the area A, a power density of

$$P' = T\ P_o/A \tag{2}$$

This power density is scattered by n molecules or atoms in a volume V = Adh, having a scattering cross section per atom C(m^2). Thus the power scattered is

$$P'' = T\ P_o\ C\ n\ A\ dh/A \tag{3}$$

where n is a number density.

The power given by (3) is scattered in all directions. If the receiver has an area A_R the power received will be

$$P_R = T\ P_o\ C^*\ n\ dh\ A_R\ T/\ h^2 \tag{4}$$

where C* is now the scattering cross section per unit solid angle or $C/4\pi$ and again we introduced the factor T to allow for the atmospheric losses from height h to the ground. Introducing dh from (1),

$$P_R = T^2\ P_o\ t_o\ C^*\ n\ A_R\ c/2h^2 \tag{5}$$

but $P_o\ t_o$ is the energy E_o of the source, and if the power P_R is received in an interval of τ seconds we have

$$E_R = T^2\ E_o\ C^*\ n\ A_R\ \Delta h/h^2 \tag{6}$$

or as the energy is proportional to the number of photons,

$$N_R = T^2\ N_o\ C^*\ n\ A_R\ \Delta h/h^2 \tag{7}$$

where Δh is now the effective height interval over which the photons are counted. Furthermore, the number of photons actually recorded is affected by the overall efficiency Q of the observing system and we get finally for the number of photons recorded, or counts, scattered from height h,

$$N_R = (n\ C^*/h^2)\ (A_R\ \Delta h\ N_o\ Q\ T^2)\ \text{counts} \tag{8}$$

Here $(A\ \Delta h\ N_o\ Q\ T^2)$ is a constant K of the equipment, h is the scattering height, C^* is the scattering cross section for the sodium atoms and n is the sodium density and thus the density may be written

$$n = \frac{N_R\ h^2}{C^*\ K}\quad \text{atoms/unit volume}$$

For our equipment we have A = 0.39 m^2, T = 0.74 and for E = 1 mJ = N_o h ν, N_o = E/h ν = $10^{-3}/(6.6\times10^{-34}\times 3\times10^{8} \times 1/5890)$ = $5890\times10^{-11}/19.8\times10^{-24} \doteq 3\times10^{15}$ photons. Assuming the efficiency of the optical system equal to Q = 0.01, for a height interval Δh = 2 km we get

$$K = (0.39)(2\times10^{3})(10^{-2})(0.74)^2\ (3\times10^{15}) =$$

$$K \doteq 1.28\times10^{16}$$

However this is only an approximation because the actual value changes with the energy of the laser pulse, and with the Q and T factors. Thus to find K, on the day in question, one compares the signal with Rayleigh scattering in the lower atmosphere.

For example, we know quite accurately the atmospheric density at 20 km, and the signal returns from this height are of the order of 25 counts for 10 laser shots (but varying from night to night), thus

$$C_R = \frac{N_A \times C_R^*}{h^2} K$$

where C_R is the number of counts for Rayleigh scattering, N_A is atmospheric number density, C_R^* is the Rayleigh scattering cross section for back-scatter and h is height.

We then have

$$K = \frac{(20\times10^3)^2\ 25/10}{N_A \times C_R^*}$$

At 20 km N_A is of the order of 2×10^{24} molecules per cubic meter and C_R^* at λ5890 $\mathring{A}$ is $1.98\times10^{-32}\times(6943)^4/(5890)^4 = 4\times10^{-32}$ and we get for K

$$K = \frac{4\times10^8(2.5)}{(2\times10^{24})(4\times10^{-32})} = 1.25\times10^{16}$$

3.2 - THE SCATTERING CROSS SECTION

By the Füchtbauer-Ladenburg formula we have that (see Appendix II).

$$\int k_\nu\, d_\nu = |(\lambda_o^2\ g_2\ n\ A_{21})/(8\ \pi\ g_1)|\ \ |1 - (n'\ g_1)/(n\ g_2)| \qquad (1)$$

The only agency responsible for the formation of excited atoms is the absorption of the light itself and thus the ratio n'/n is exceedingly small, of the order of 10^{-4} or less. Thus we have simply

$$\int k_\nu\, d_\nu = (\lambda_o^2\ g_2\ n\ A_{21})/(8\ \pi\ g_1) \qquad (2)$$

or in terms of the integrated cross section

$$\int C_\nu \, d_\nu = (\lambda_0^2 \, g_2)/(8 \, \pi \, \tau \, \, g_1) \tag{3}$$

where $\tau = 1/A_{21}$

Formula (2) above is sometimes written in a different way, introducing the so called f value.

In the classical electron theory of dispersion, the optical behavior of n atoms per unit volume was represented by the behavior of N quasi-elastically bound electrons, or the dispersion electrons. The ratio N/n was found to be constant for a particular spectral line and was denoted by f. In quantum theory the f value is inversily proportional to the lifetime of the resonance line.

$$f \, \tau = (\, m \, c \, g_2 \, \lambda_0^2)/(\, 8 \, \pi^2 \, e^2 \, g_1) = \tag{4}$$

$$= 1.51 \, g_2 \, \lambda_0^2/g_1$$

Introducing the f value in (2) we have with $g_2 = g_1$.

$$\int k_\nu \, d_\nu = \frac{\pi \, e^2}{m \, c} \, n \, f. \tag{5}$$

From equation (3) we are able to calculate the integral of the scattering cross section. We only need the τ value. Some constants for the sodium D lines are given below.

TABLE III

SOME CONSTANTS FOR THE D LINES

	g_2/g_1	λ_o(Å)	f value	g(ph/sec/atom)	$\tau = 1/A_{21}$
D_2	2	5890	0.67	0.797	16×10^{-9} sec
D_1	1	5896	0.33		

We have then for the D_2 line, an integrated absorption cross section of

$$\int C_\nu \, d\nu = [(5890)\times 10^{-10}]^2 \times 2(8\,\pi \times 16\times 10^{-9})^{-1}$$

$$\int C_\nu \, d\nu = 34.6 \times 10^{-14}/(4 \times 3.14 \times 16 \times 10^{-9})$$

$$\int C_\nu \, d\nu = 1.72 \times 10^{-6} \text{ m}^2 \text{ sec}^{-1}$$

and for D_1,

$$\int C_\nu \, d\nu = 0.86 \times 10^{-6} \text{ m}^2 \text{ sec}^{-1}$$

Actually we are interested in the effective resonance scattering cross section of an atom which is given by the integral of the product of the absorption cross section and the distribution of photons in frequency

$$C_{eff} = \int C_\nu \, g_\nu \, d\nu \, ,$$

Where

$$g_\nu = \frac{I_\nu}{\int I_\nu \, d\nu}$$

The largest possible value of C_{eff} will be obtained when the bandwidth of the laser output is much less than the bandwidth of the atmospheric sodium doppler bandwidth. The maximum for the scattering cross section is of the order of 10^{-15} m^2 for the D_2 line and 5×10^{-16} m^2 for the D_1 line.

For our tuning system, the bandwidth is of the order of 5 pm at the D_2 line so that our C value is 4×10^{-16} m^2.

3.3 - TUNING OF THE LASER SPECTRUM

The dye laser available has a spectral bandwidth of about 150 Å. We want only a very narrow band centered at the D_2 line because the narrower the bandwidth, the larger will be the value of the scattering cross section.

Tuning to the D_2 line is accomplished by means of three tilted Fabry-Perot mode selectors. (See Appendix IV).

For two of the tuning elements, we used two pairs of dielectric coated mirrors, flat to $\lambda/20$ and with a reflection coefficient (for power) R = 0.5. The mirror holders were constructed at INPE's work shop. Mylar rings act as spacers to obtain etalons of 120 Å and 17 Å free spectral range. The parallelism adjustments are made through light spring pressure through three adjusting screws. The third mode selector is a Coherent Optics Inc. tunable model, with a free spectral range of 2 Å.

The tunable etalon of 2 Å free spectral range, varies the distance between its mirrors, through application of a voltage on a piezoelectric crystal. The presence of this crystal element makes the instrument very sensitive to temperature changes. Therefore a temperature stabilizing circuit was constructed for each etalon.

The circuit consists of a temperature sensor (an AC 127 transistor), an amplifier and a heating resistor made of thin copper wire. The heating element is coiled around the mirror holders and the sensor is in good contact with the metal. The idea is to maintain the system at a level above room temperature with sufficient sensitivity to balance external temperature variations. The circuit is shown in figure 10. The etalons are covered by styrofoam covers which in turn are covered by metallic shields.

A sodium lamp furnishes a reference and a photomultiplier tube indicates when the etalons are in the position of maximum transmission.

The sodium lamp light is collimated, enters the resonant cavity passing through the three etalons, is reflected at the end mirror with total reflection and passes again through the etalons and is directed on the sensitive area of the PMT. The introduction of the sodium lamp light into the cavity and from the cavity upon the photomultiplier tube is made by a right angle prism which can be introduced in the optical path of the resonator at a proper position. The sodium lamp is situated at one side of the optical path and the PMT at the other. The sodium lamp light enters the diagonal face of the prism, is internally reflected at one of the right angle faces and emerges through the other face from where the light is then reflected to the PMT aperture, after its double passage through the etalons. This arrangement is shown

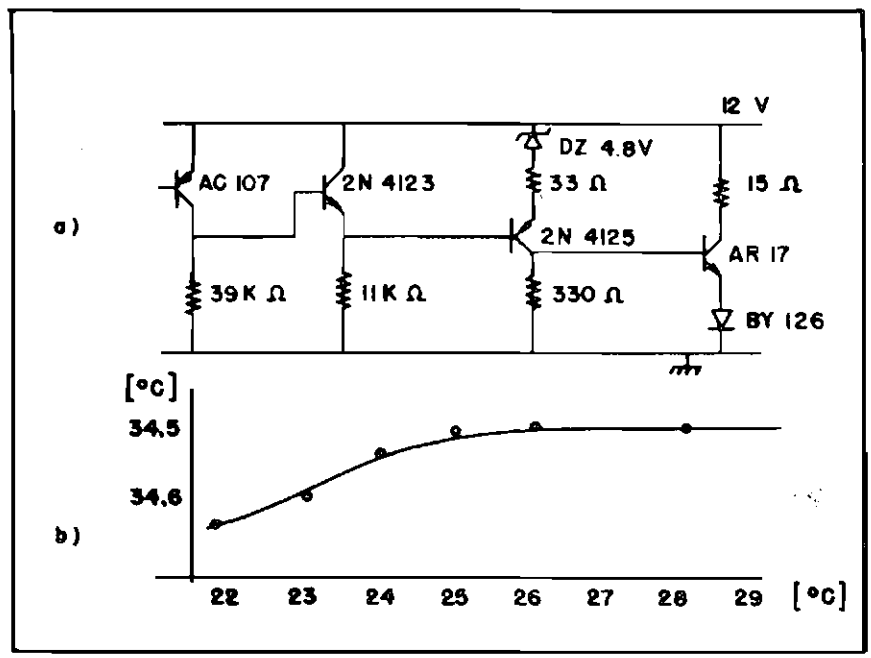

Fig. 10 - Temperature control

a) Circuit

b) Performance:

Stabilized vs. external

temperature

in figure 11. The alignement of sodium lamp, prism and PMT was done using a Helium-Neon laser and then fixed.

For the measurement of wavelength we used a grating spectrometer. Its output can be observed visually or may be photographed on polaroid film. Between the collimating lens and the grating, it is possible to insert a tunable Fabry Perot etalon (Coherent Optic's model 370), thus increasing the resolution of the system up to 0.02 Å per mm. The bandwidth of the laser line measured with this system is 5 pm.

A detailed description of the tuning system has been given by *Clemesha and Kirchhoff* (1972).

The tuning procedure is then as follows.

With the etalons out of the resonant cavity we check the spectral output of the laser with the spectrometer. We want a spectral output covering the sodium D lines. Responsible for this is the dye concentration in the ethanol. We found the adequate concentration to be 0.8×10^{-4} mol per liter of ethanol. We then check the parallelism of the etalons, making adjustments if necessary. With the etalon of 120 Å free spectral range in the cavity and beginning with zero tuning angle we increase this angle up to a maximum indication from the PMT. The same is done with the etalon of 17 Å free spectral range. The last etalon is placed at a small angle only to avoid reflections, because the tuning of

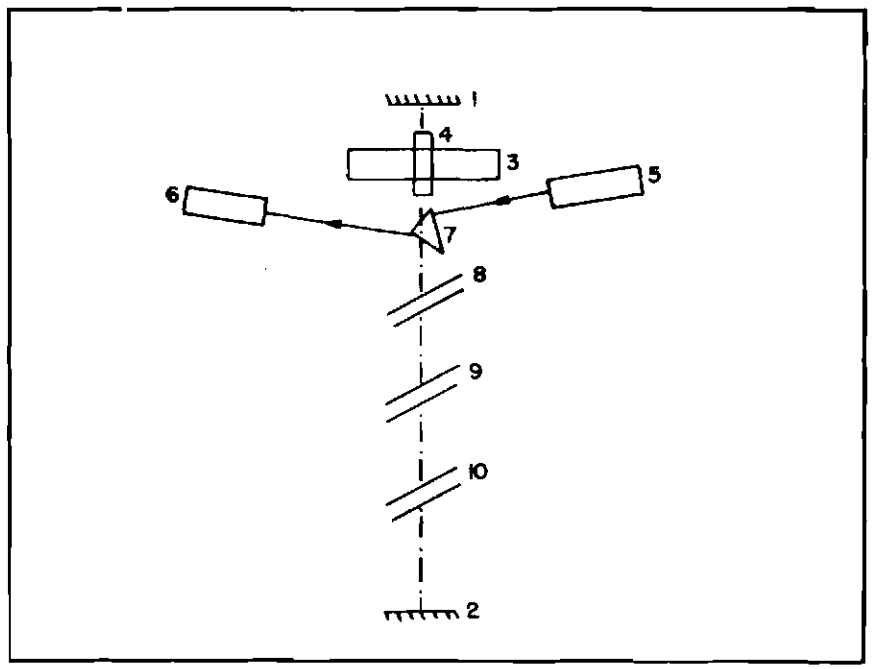

Fig. 11 Dye laser lay out

1 - Output mirror R = 50%
2 - Total reflection mirror
3 - Capacitor unit
4 - Flash lamp - dye cell windows
5 - Sodium lamp and collimator
6 - Photomultiplier tube
7 - Right angle prism
8, 9 and 10 - Fabry Perot units

this unit is done electronically. Since all etalons are at the right position, the laser output is tuned to the D_2 line; the laser line of the spectrometer output will be superposed on the D_2 reference line.

As the system comprises a great number of variables which must be controlled simultaneously, tuning is a delicate and long procedure when some misalignement occurs in the system. However, once a good alignement was made, the system shows a very good stability remaining aligned for more than three months, and to make a measurement only the tuning filters must be checked and their position optimized.

Actually the tuning of the laser output to the D_2 line with a bandwidth of only 0.05 Å is the result not only of the installed mode selectors but is also the consequence of multiple reflections in elements such as the dye cell windows, if they are plane and parallel. In this case, as reported by *Gibson* (1969), the final tuning must be accomplished by varying the temperature of the dye solution. For our system, in order to not increase the number of elements to be controlled, we wedged the 50% mirror at 1^o, using it as one of the windows, and made an anti reflection coating on the other dye cell window also with a 1^o wedge.

3.4 - DYE LASER PERFORMANCE

After the tuning system was mounted we felt that the irregularity in the laser beam intensity was becoming a problem for the exact determination of the laser bandwidth. This irregularity in both intensity and divergence is a characteristic of the kind of excitation used. After a number of shots, the coaxial flash lamp deteriorates becoming opaque in a non uniform way. (This coaxial flash lamp dye laser was previously constructed by *Motisuke* (1970)). Also the dye solution deteriorates after a number of shots. Thus substitution of the glass tubes and dye solution was supposed to remove in part the problems of intensity irregularity and sometimes even failure of laser action. However, the problems remained and laser action became more difficult.

An article conducted by *C. L. Stong* (1970), warns against the use of plastic tubing for the flow of dye because *"most plastics contain an oily plasticizer which may contaminate the solution preventing laser action"*. Although plastic tubes were used since the beginning, when contamination was not noticed, we changed to rubber tubes. New dye solution was used and the laser was carefully aligned but only the first two or three firings showed laser action. The laser action then ceased completely. The situation was obviously worse and we came back to the plastic tubes.

At this time the laser output was very weak, from 1 to 2 mJ, irregular, and from three lamp discharges, only one produced lasing.

Continuing to look for a reason of the contamination, it was decided to measure the absorption characteristics of the dye. We then measured the absorption characteristics of fresh dye solution and compared with solution already used in the dye laser. The absorption curves using both ethanol and methanol are shown in figures 12 and 13. For comparison, the same curve is shown in figure 14 after *Weber and Bass* (1969).

In our curves, ordinate units are absorbance, defined as $A = \log I/I_0 = kd/2.3$ where d is distance and k the absorption coefficient. To compare the ordinate values, for the ethanol we have at the peak of the curve A = 1.5, and the d value was 1 cm, thus k = 1.5 cm^{-1} or taking the dye concentration into account we have

$$k' = 2.3 \times 1.5/(1.8 \times 10^{-5}) = 2.3 \times 83 \times 10^3 \text{ cm}^{-1}/\text{mole/liter}$$

Thus the curve coincide in frequency but the ordinate values differ by a factor of about 2.3. We were unable to explain this difference.

Three things remained to be checked: the tubes, the ethanol and possibly, even the dye. The tubes because of the reasons given by *Stong*, the ethanol because we then used "pure" alcohol from a different origin than before, and the dye because ours, from J.T.Baker,

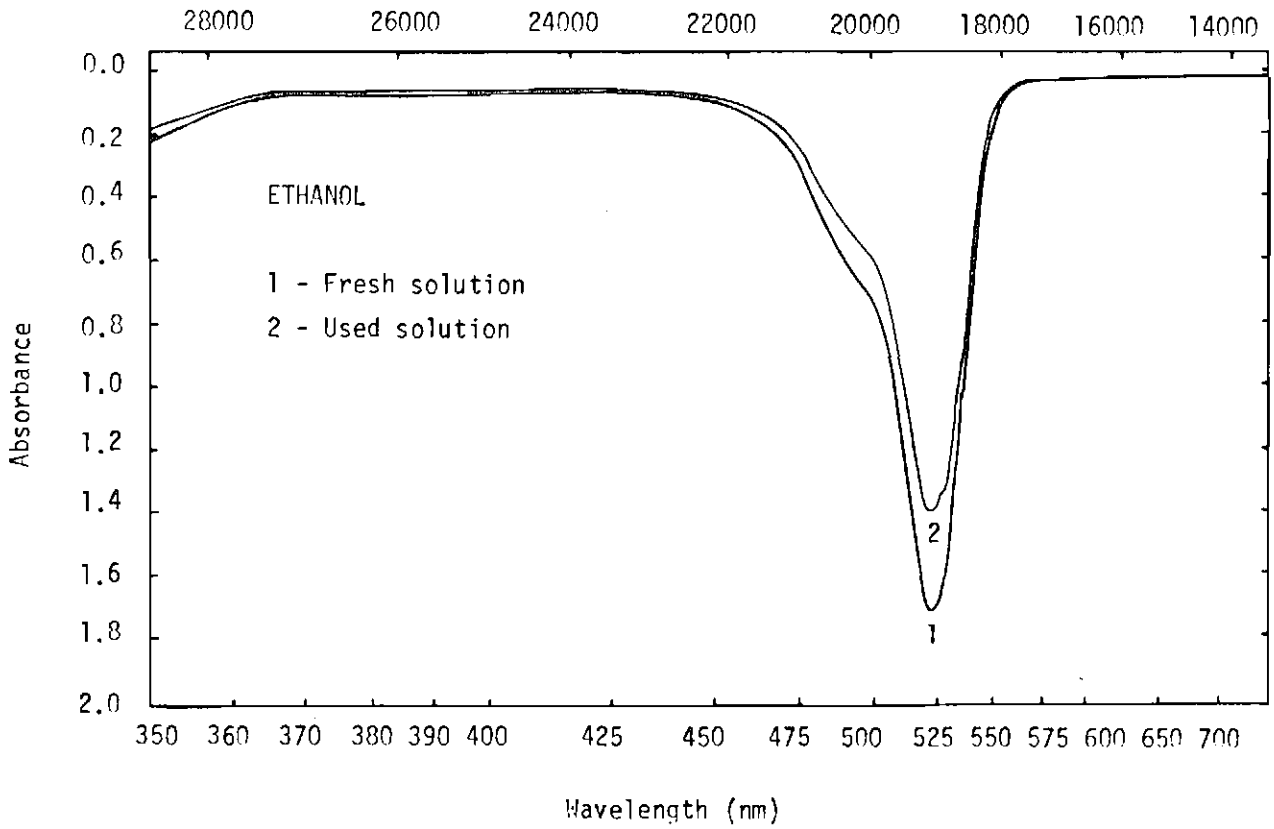

Fig. 12 ABSORPTION CURVES

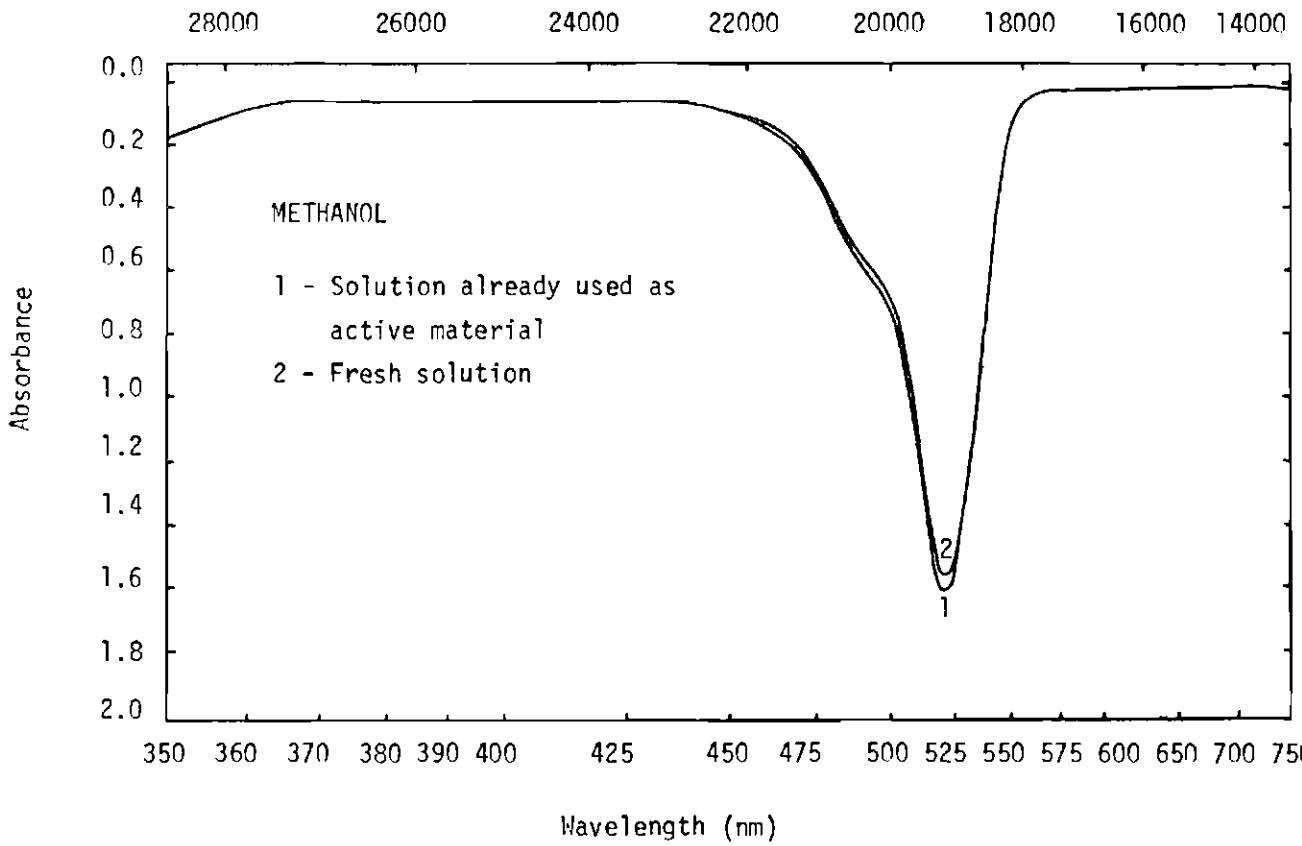

Fig. 13 ABSORPTION CURVES

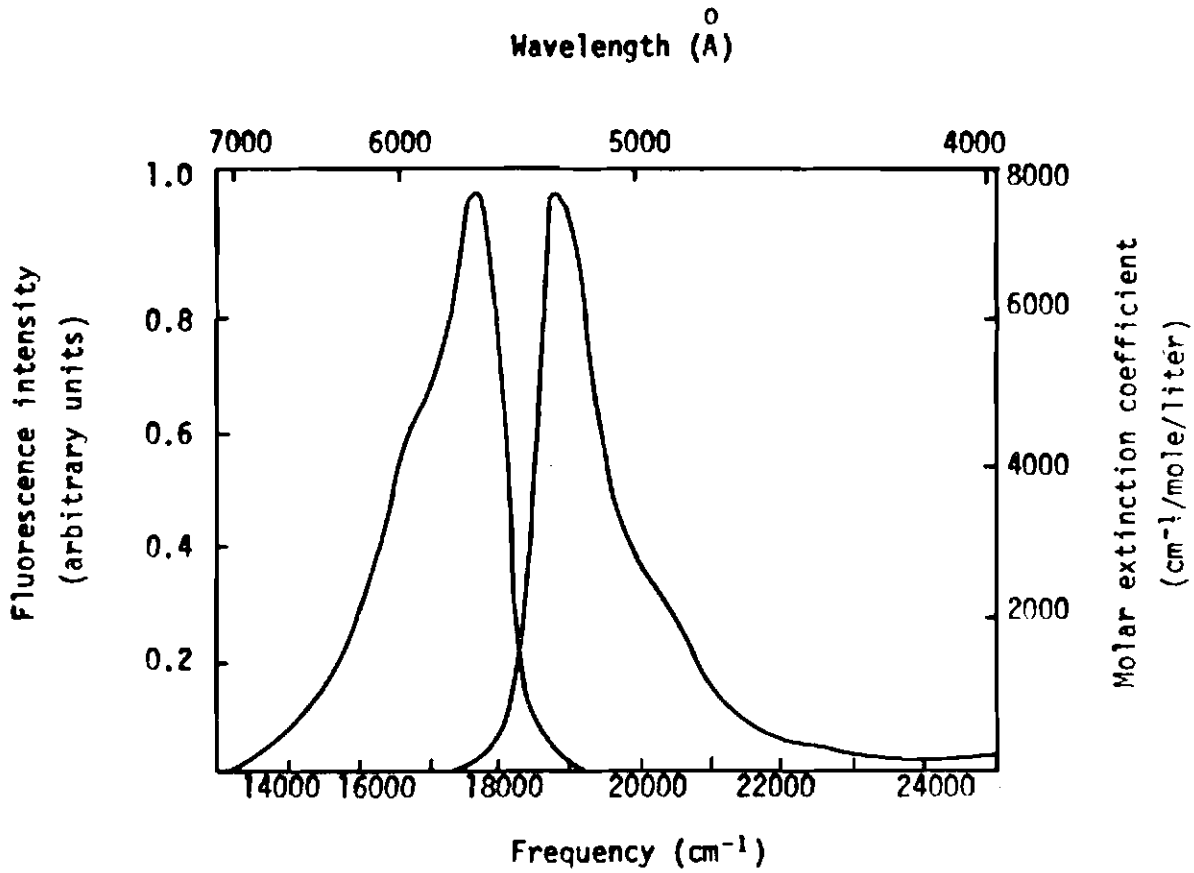

Fig. 14 - Absorption and fluorescence spectra of 10^{-4} M Rhodamine 6G in ethanol. (After ..eber and Bass).

has a molecular weight of 479 which is somewhat different from 449 given in the same article by *Stong*. (The reason may lie in the fact that our formula for the Rhodamine 6G has also one Cl atom whereas the structure shown by *Peter Sorokin* (1969) has not.)

First, copper tubes were installed and we changed to a better grade of ethanol. With these changes the contamination due probably mainly to the inadequate quality of the ethanol used before was removed.

In between, we also decided to substitute the coaxial flashlamp dye laser for an eliptical cavity, because this configuration is easier to handle and has better beam divergence characteristics. This dye laser properly tuned has an output of about 3 mJ in a pulse of 0,5 μsec (*Kirchhoff*, 1971) and may be used in repetition rates of 10 pulses per minute.

The tubes for the dye flux were changed for teflon and stainless steel and the pump is actuated magnetically.

3.5 - THE EXPERIMENT

The basic ruby radar generally measures density profiles above 30 km. For our experiment we have to begin at a lower height for calibration purposes. However at lower heights the signal due to Rayleigh scattering is so strong that the preamplifier saturates entering into oscillation.

To overcome the problem, we used the receiving rotating shutter facilities. The shutter furnishes a 4 volts positive, 20 μsec pulse a little after closing the receiving aperture. It then remains closed for about 130 μsec. This is the time necessary for the light to travel twice a distance of about 20 km, and as we want a reference Rayleigh signal from 20 km, this time must be diminished. For the signal to be measured beginning at, say 15 km, a delay of 30 μsec for the shutter pulse is adequate. Thus delaying this pulse for 30 μsec, and then using it to fire the laser, the strong signal from the first 15 km is prevented from entering the receiver.

The trigger circuit is shown in figure 15.

The measurement is made in groups of ten laser firings after which the tuning and the Rayleigh signal at the reference level is checked, to assure that no clouds are present in the optical path. For each sequence of a hundred firings, the LASNA program plots a sodium density profile, and if more data is available a mean for the night is also deduced.

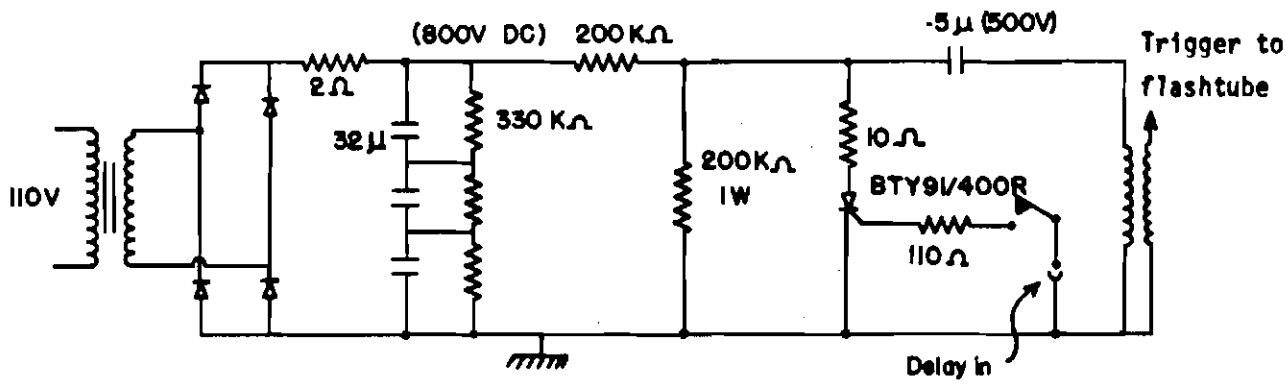

Fig. 15 - Dye laser trigger

3.6 - LASER RADAR RESULTS FOR MARCH 1972.

The first reliable measurements were made on March 18, and since then, measurements have been made on almost every night of clear sky. On March 18, measurements lasted for about two hours. This night showed the least values of both density and abundance measured in this period.

Figure 16 a and b shows respectively the mean abundance and density values for the days in question. At least three of the nights showed a second density maximum which we will call peak II, near 86 km. It appears on March 25, 27, 29, and even three peaks are seen for 27, showing another maximum at 102 km. The similarity in shape of these three density profiles is remarkable (figure 17). Although this bifurcation of the layer disappears for the average month profile, because the peaks are not at the same height for each day, a vestige of the event still exist for the March profile at 86 km. The average profile for the eight measurements of March 1972 is shown in figure 18. The topside scale height is less than 2 km at 98 km, a common feature for all the March nights on which measurements were made.

Height variations of peak I from night to night are shown in figure 19 a, and the height variations for each night in figure 19 b.

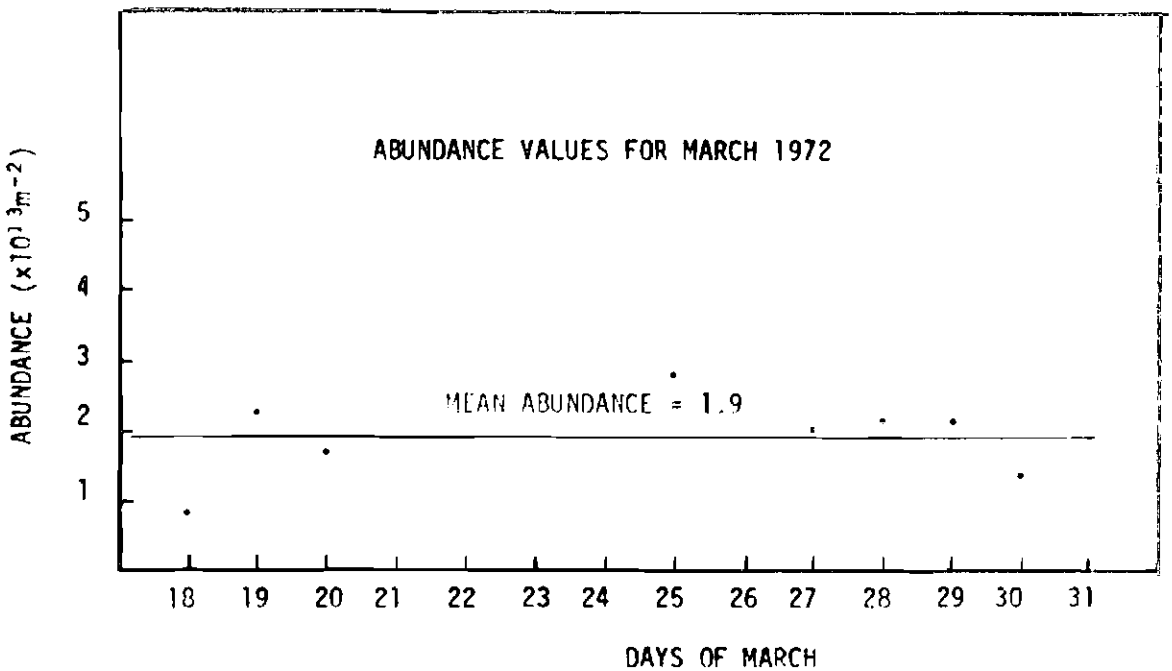
ABUNDANCE VALUES FOR MARCH 1972
ABUNDANCE (x10^{3}m^{-2})
MEAN ABUNDANCE = 1.9
1
2
3
4
5
18 19 20 21 22 23 24 25 26 27 28 29 30 31
DAYS OF MARCH

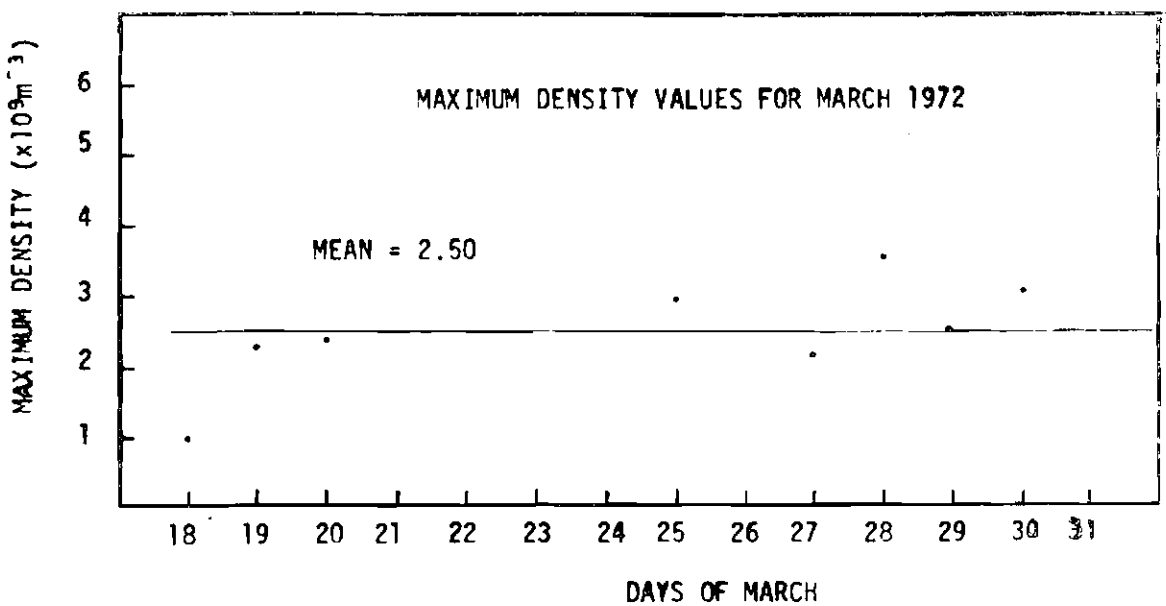
MAXIMUM DENSITY VALUES FOR MARCH 1972
MAXIMUM DENSITY (x10^{9}m^{-3})
MEAN = 2.50
1
2
3
4
5
6
18 19 20 21 22 23 24 25 26 27 28 29 30 31
DAYS OF MARCH

Fig. 16

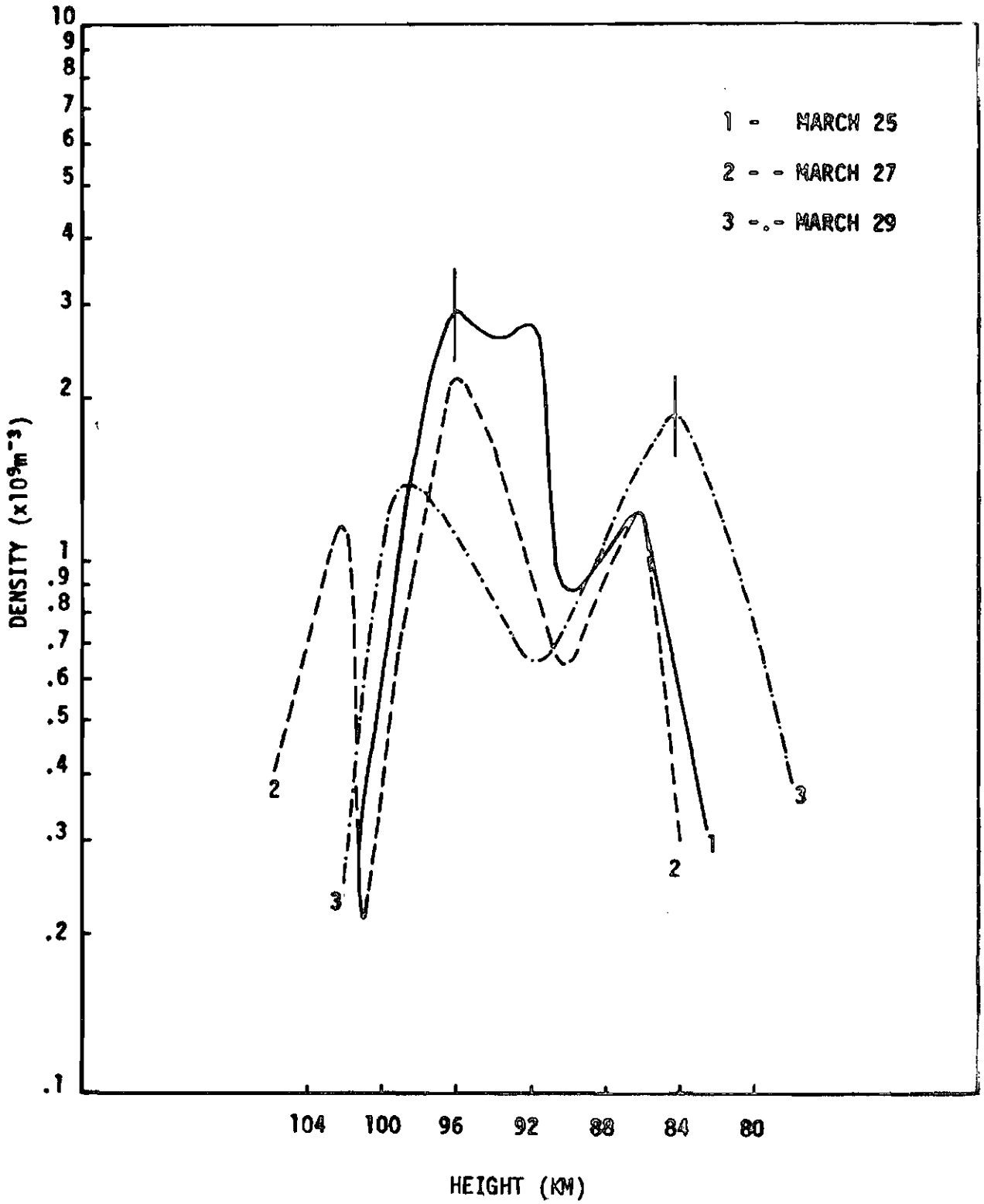

Fig. 17 - Density profiles for March 25, 27 and 29

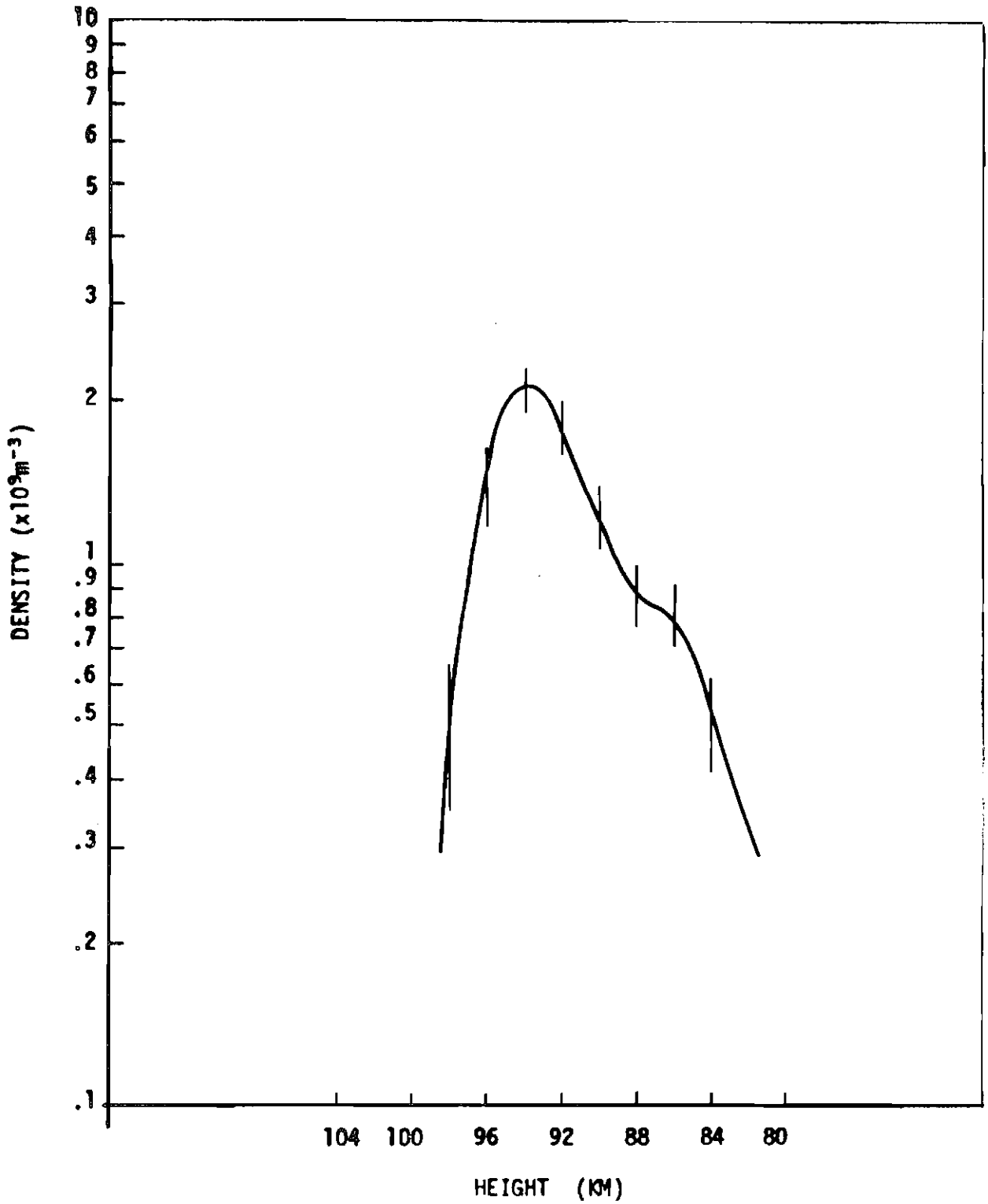

Fig. 18 - Mean for March 1972

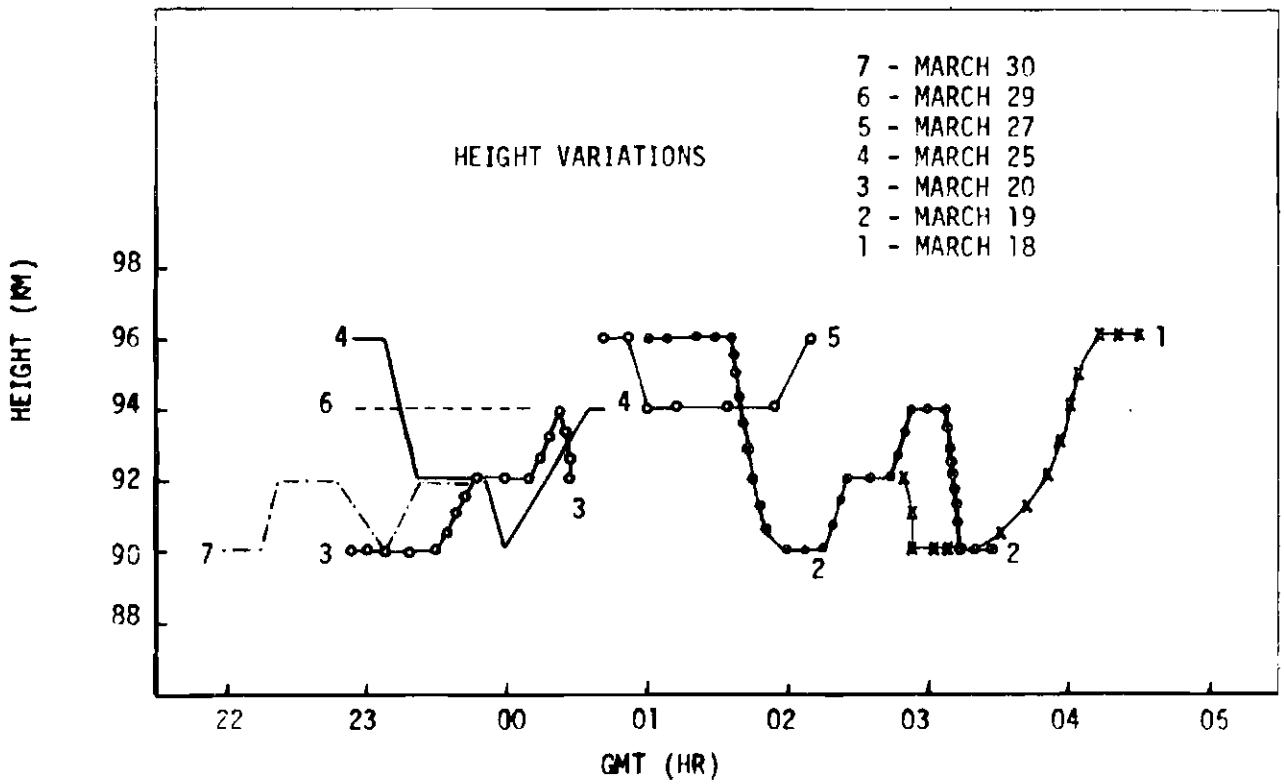
HEIGHT VARIATIONS
7 - MARCH 30
6 - MARCH 29
5 - MARCH 27
4 - MARCH 25
3 - MARCH 20
2 - MARCH 19
1 - MARCH 18
HEIGHT (KM)
98
96
94
92
90
88
22
23
00
01
02
03
04
05
GMT (HR)

(a)

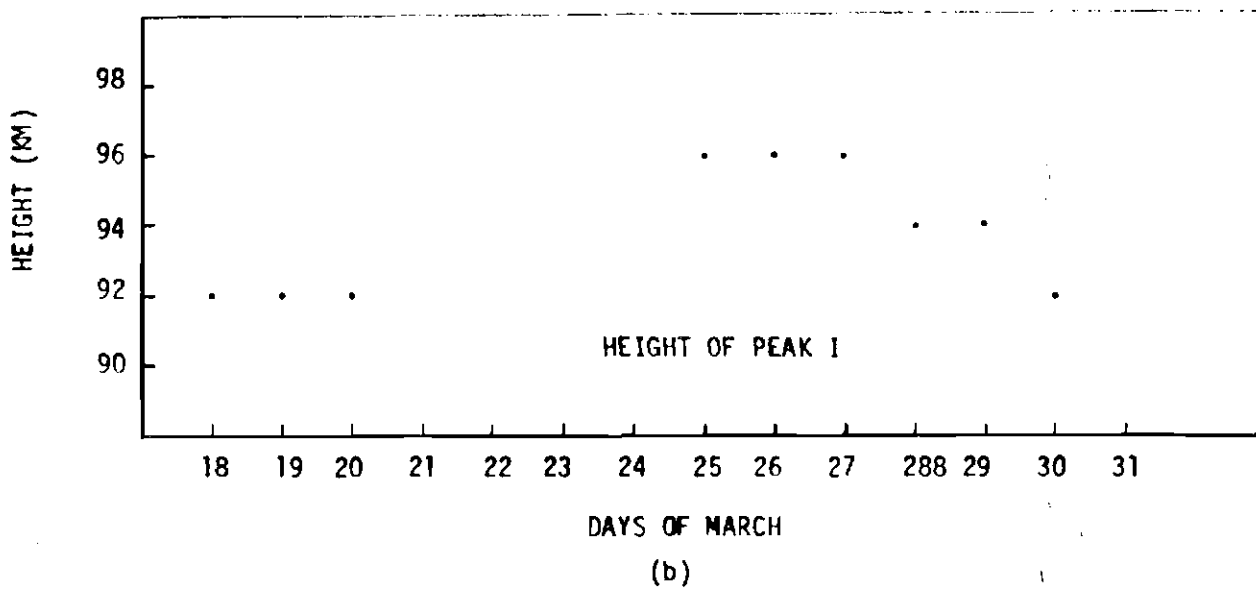
HEIGHT (KM)
98
96
94
92
90
HEIGHT OF PEAK I
18
19
20
21
22
23
24
25
26
27
288
29
30
31
DAYS OF MARCH

(b)

Fig. 19

3.7 - LASER RADAR RESULTS FOR APRIL 1972

The mean abundance and maximum density values for April 1972 are shown in figure 20, a and b. On the first two days, a density maximum near 101 km was again detected (figure 21) and peak II at the lower heights, near 86 km, appeared at least on six nights. Again it is interesting to note the similarity in shape for subsequent nights (figures 22 and 23). On April 19, a quite different shape was recorded (figure 24). The average April profile (figure 25) is very similar to the March profile showing also a vestige of peak II near 86 km. Figure 26, a and b, shows the variation with height during each night and the variation from day to day.

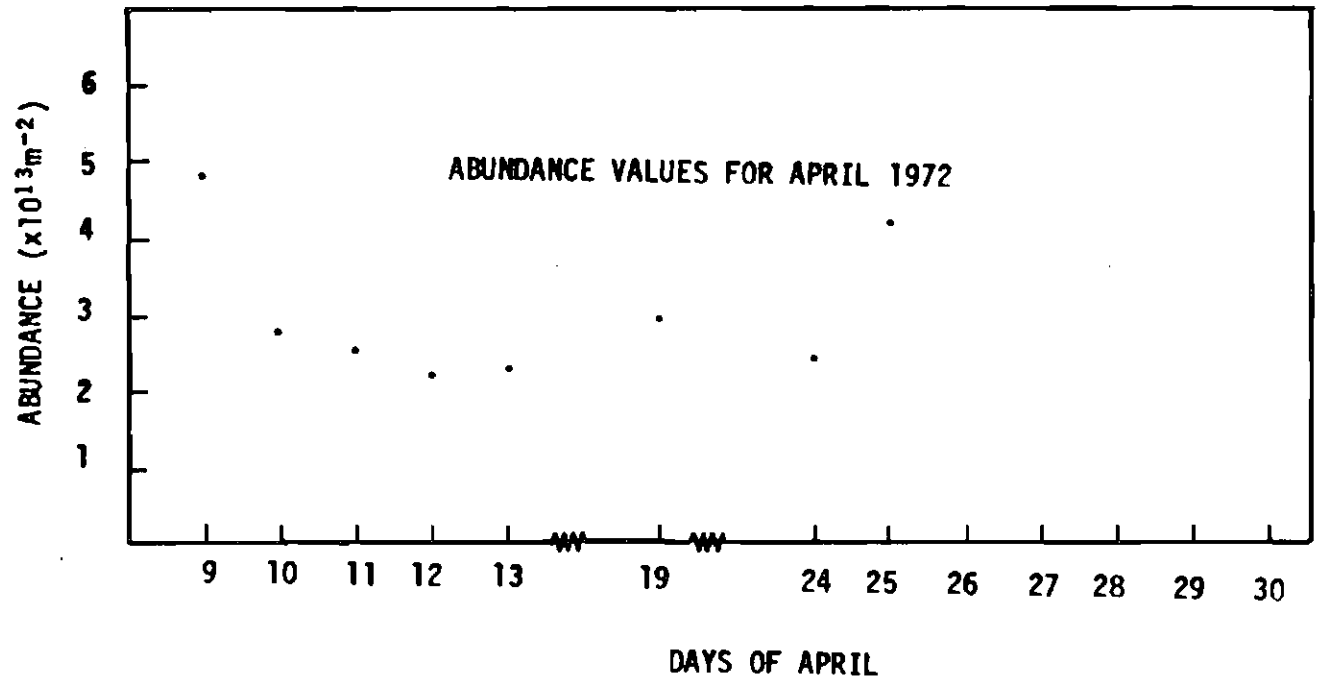
ABUNDANCE VALUES FOR APRIL 1972
ABUNDANCE (x10^{13}m^{-2})
1
2
3
4
5
6
9
10
11
12
13
19
24
25
26
27
28
29
30
DAYS OF APRIL

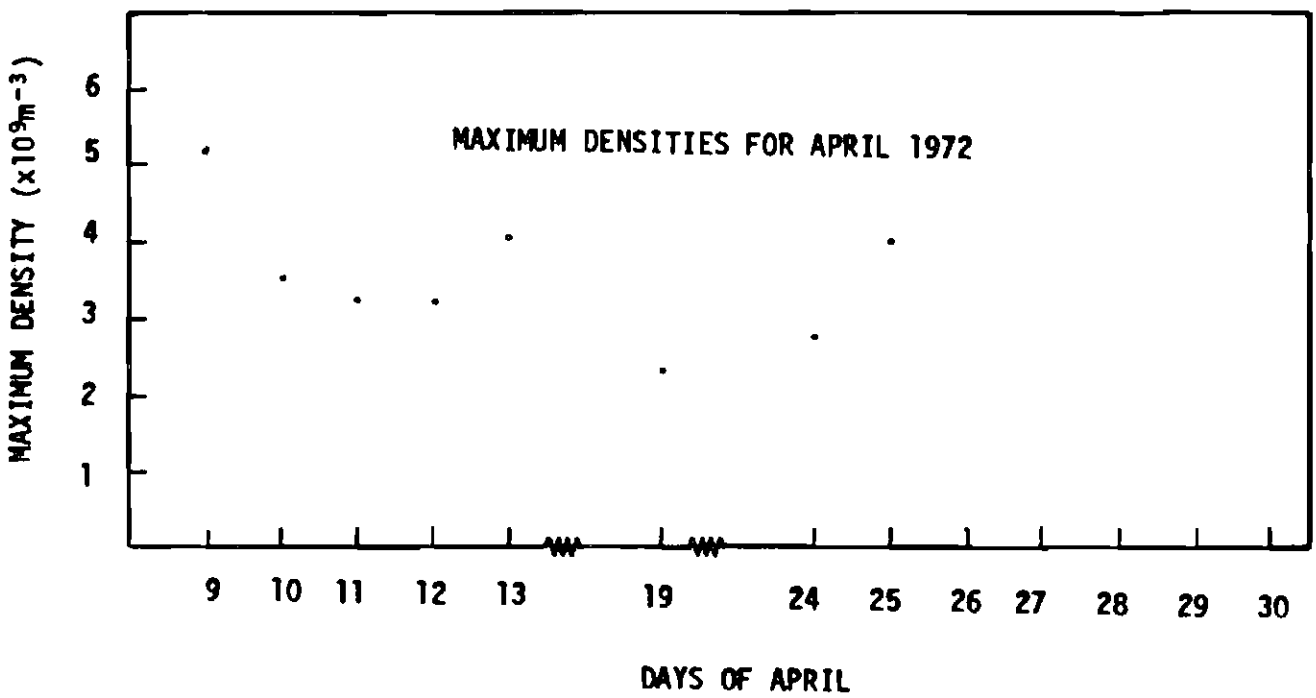
MAXIMUM DENSITIES FOR APRIL 1972
MAXIMUM DENSITY (x10^{9}m^{-3})
1
2
3
4
5
6
9
10
11
12
13
19
24
25
26
27
28
29
30
DAYS OF APRIL

Fig. 20

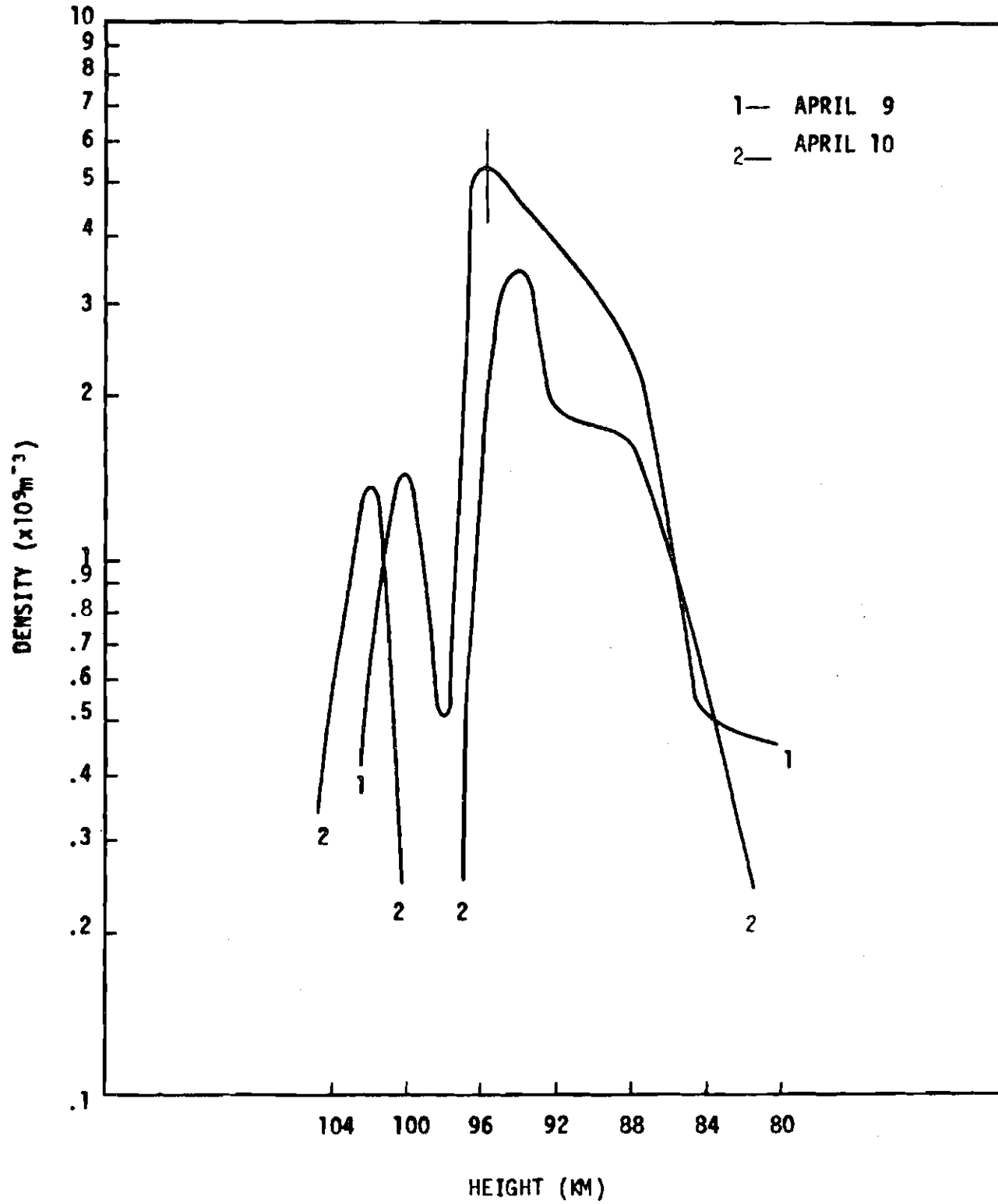

Fig. 21 - Secondary sodium layers near 101 km

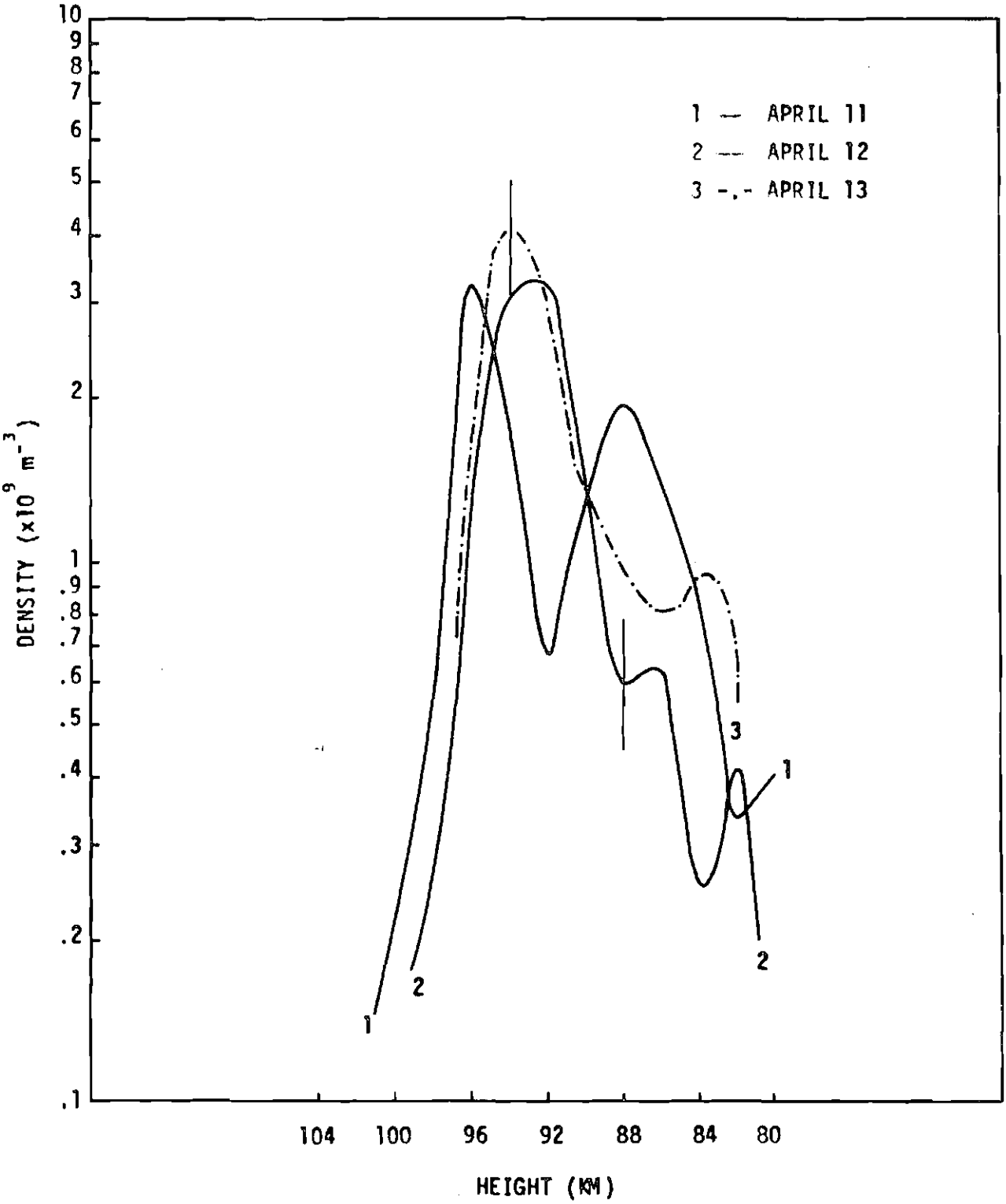

Fig. 22 - Density profiles showing shape similarity

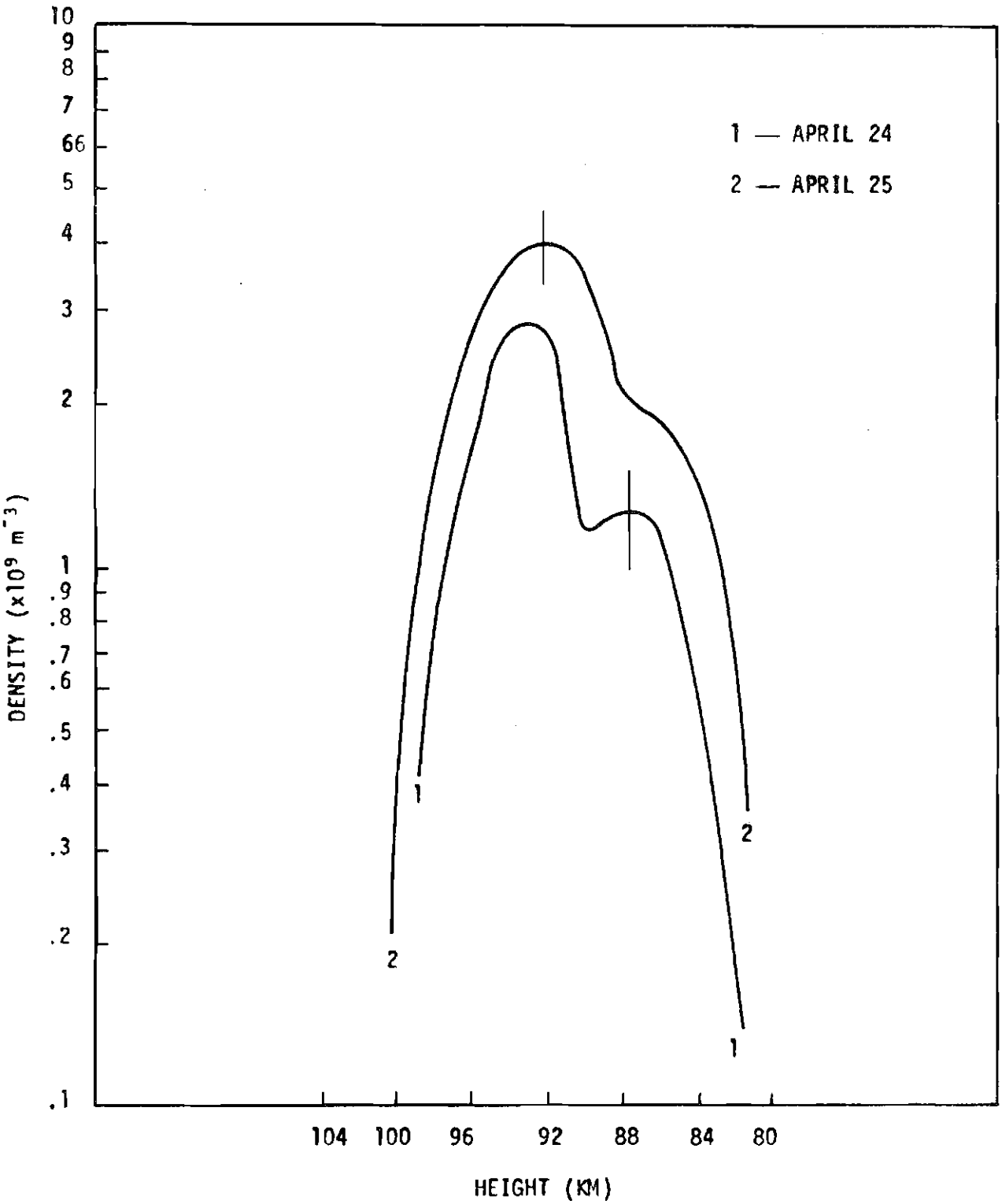

Fig. 23 - Density profiles showing shape similarity

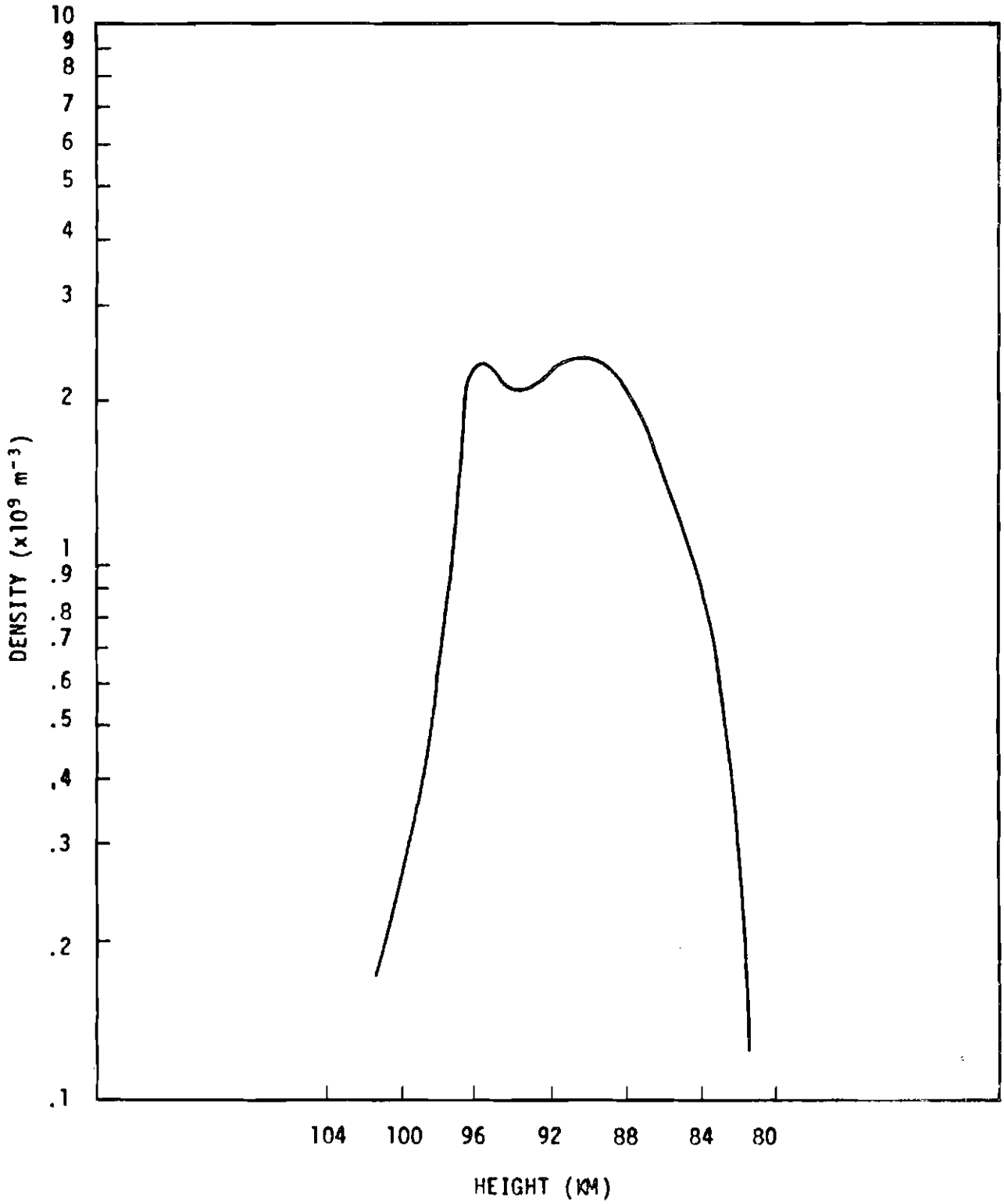

Fig. 24 - Density profile for April 19, 1972.

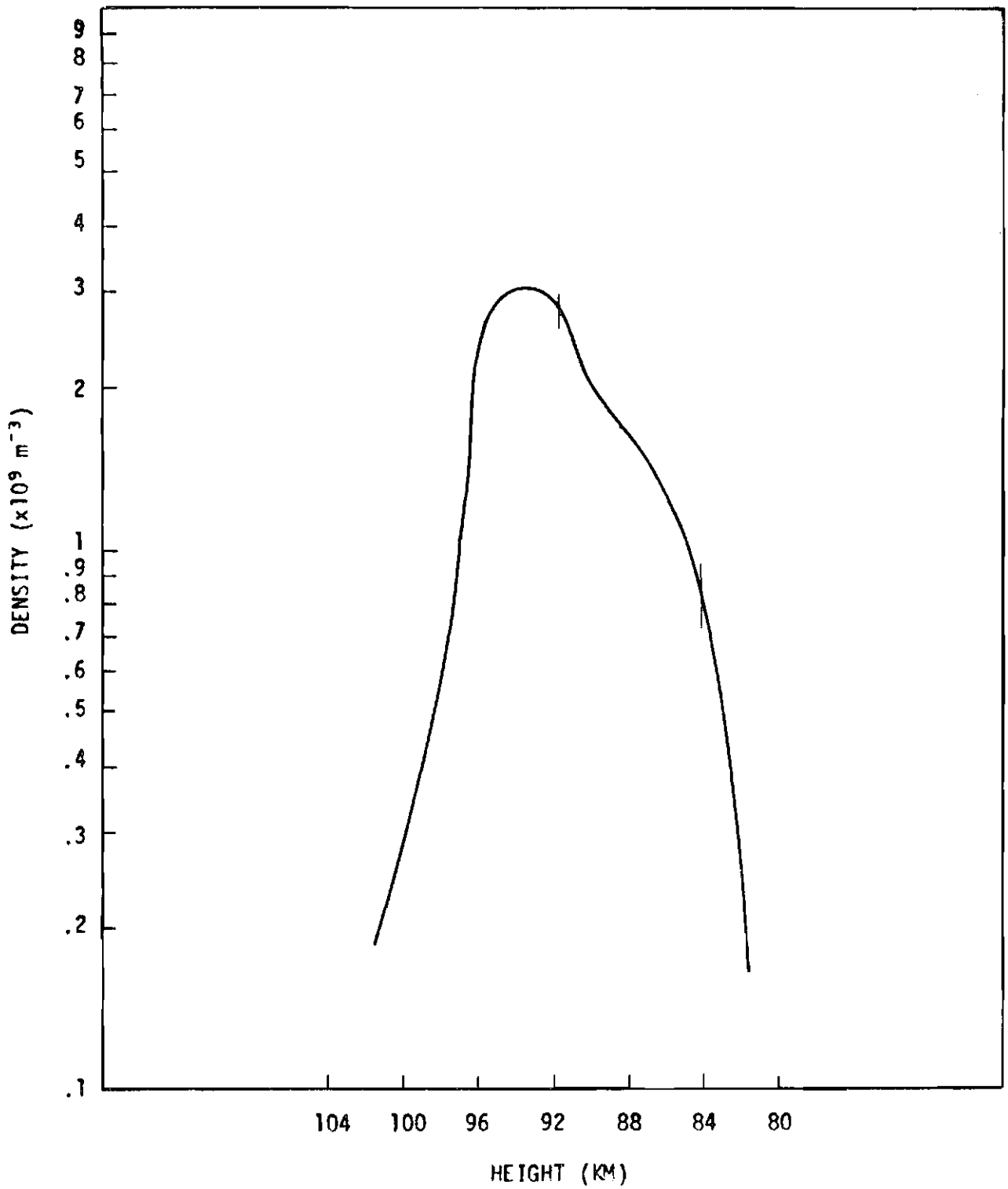

Fig. 25 - Mean for April 1972.

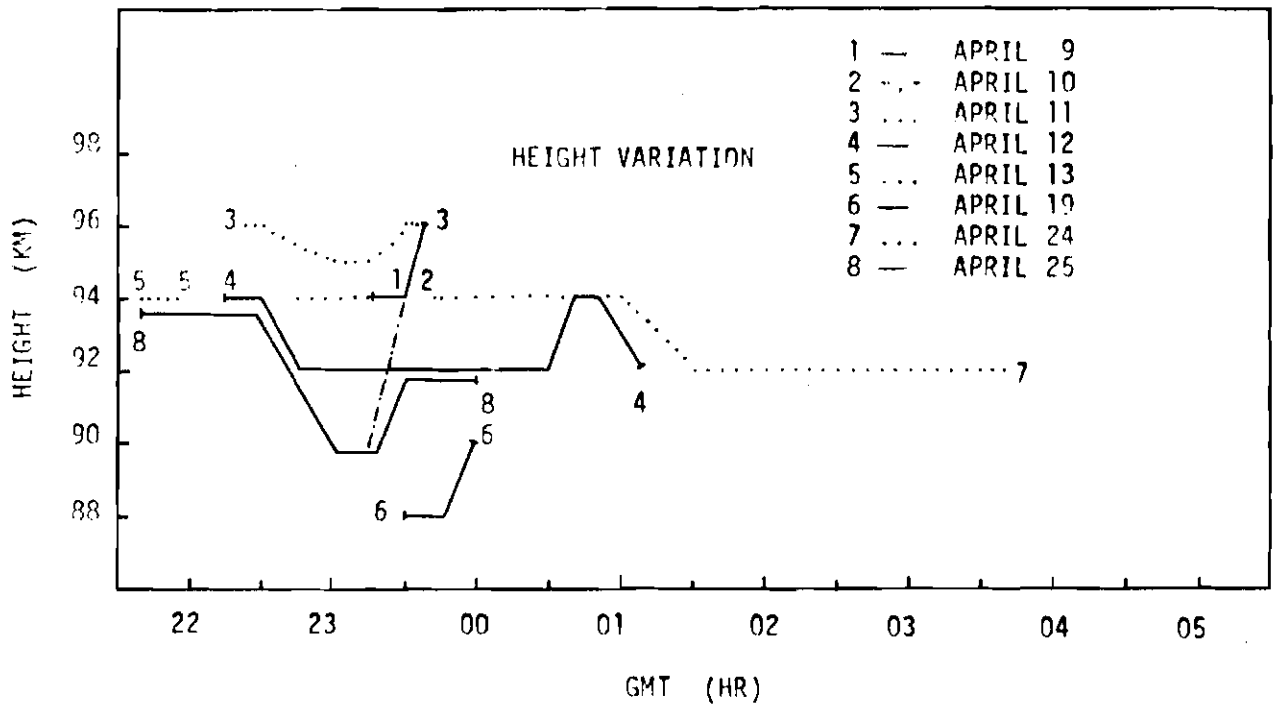
HEIGHT VARIATION
1 — APRIL 9
2 -.- APRIL 10
3 ... APRIL 11
4 — APRIL 12
5 ... APRIL 13
6 — APRIL 19
7 ... APRIL 24
8 — APRIL 25
HEIGHT (KM)
98
96
94
92
90
88
22
23
00
01
02
03
04
05
GMT (HR)

(a)

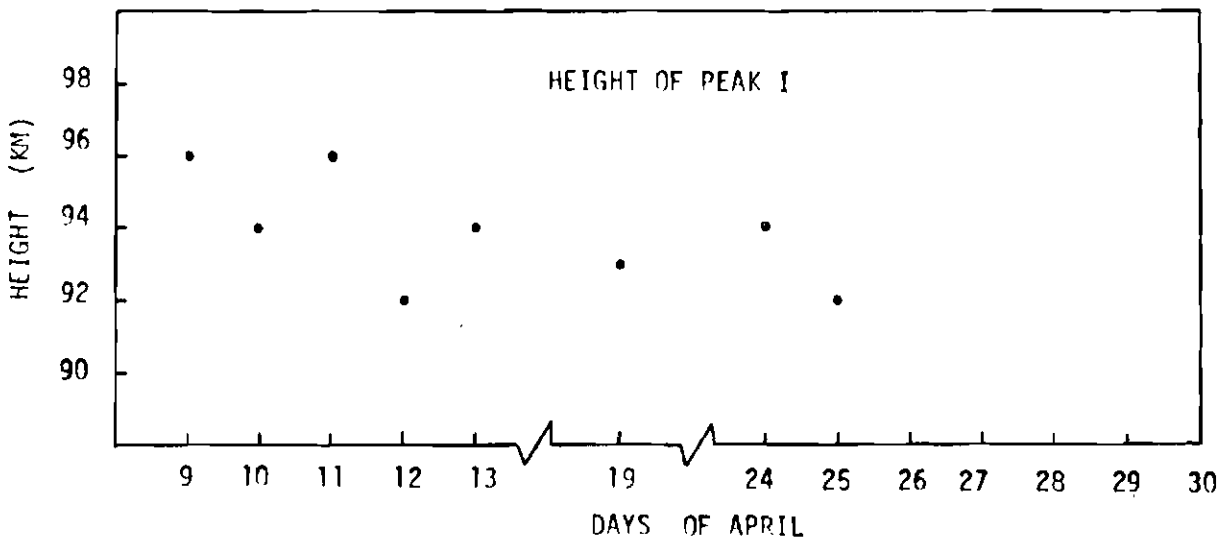
HEIGHT OF PEAK I
HEIGHT (KM)
98
96
94
92
90
9
10
11
12
13
19
24
25
26
27
28
29
30
DAYS OF APRIL

(b)

Fig. 26

3.8 - TWILIGHT SODIUM PROFILES

Weather conditions were rather bad during the twilight periods and thus only seven twilight profiles were possible to deduce. The shape of the profiles is given in figure 27 and a table of abundance and maximum density values is given in Table IV. It appears that the abundance values deduced from the twilight data are somewhat greater than the ones deduced later in the night and that the height of the maximum density for the twilight data is somewhat lower.

Gibson and Sandford (1971), point out that the seasonal variation of the altitude of the peak of the layer at night is different from that previously reported for twilight. Thus a comparison of data values over short periods becomes more difficult. Furthermore, twilight measurements are obtained in only a few minutes, and thus will be more seriously affected by short period fluctuations. It seems likely, therefore, that only measurements over long periods may be of some help in making comparisons with the night time data.

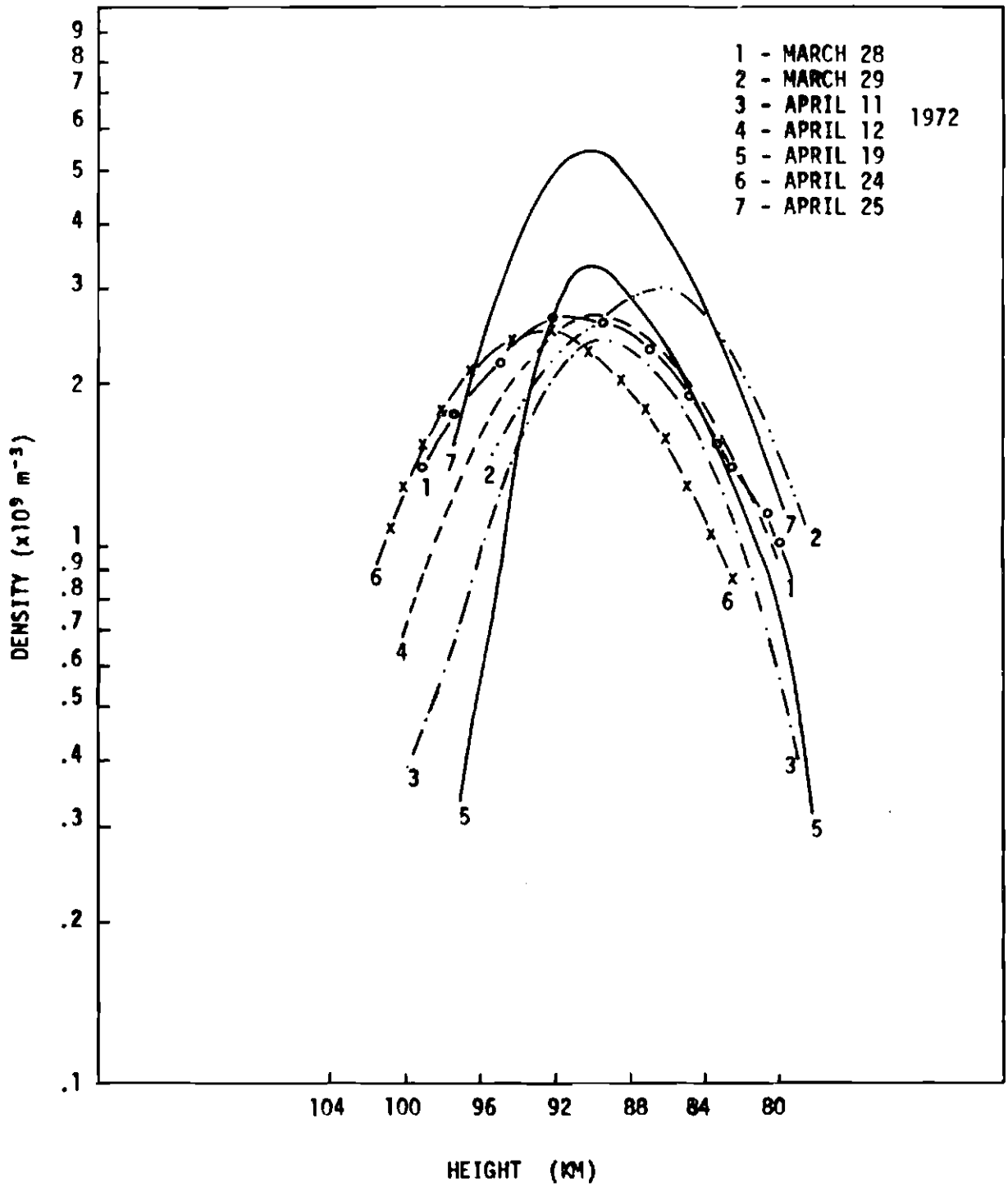

Fig. 27 - Some twilight profiles

TABLE IV

TWILIGHT/LASER RADAR COMPARISON

DATE 1972		ABUNDANCE FOR		DENSITY AT PEAK I		PEAK AT KM	
Month	day	Twilight	Radar	Twilight	Radar	Twilight	Radar
3	28	4.0	2.16	2.7	3.60	92	94
3	29	4.1	2.12	3.0	2.49	88	94
4	11	3.3	2.85	2.4	3.25	89	96
4	12	3.8	2.27	2.7	3.24	90	92
4	19	2.3	2.92	3.3	2.35	89	92
4	24	3.8	3.15	2.5	2.74	92	94
4	25	5.3	4.18	5.4	3.96	90	92

3.9 - DISCUSSION AND CONCLUSIONS

Atmospheric sodium data for a period of two months were presented. Although this amount of data is still insufficient in some aspects, it is enough to show that the process of taking the data is reliable. Thus the main task of this work was achieved.

To our knowledge, the only other station measuring atmospheric sodium using a laser radar is Slough, England, in the Northern Hemisphere. Thus we will compare our results with this station (see references 4, 19, 20, 33).

Three features call our attention. First, it seems that the topside scale height of our profiles is less than that reported. All of our profiles have a scale height very near to 2 km, at 98 km, meanwhile the reported values at this altitude are very near to 4 km.

Second, a great similarity in shape of the profiles from day to day is apparent, for some adjacent nights. This is interesting to note taking into account the considerable variations which occur within the period of one night. About this, *Gibson and Sandford* (see references above) make no comments.

Third, a secondary layer near 102 km was detected on three nights during the 2 months of observation, while *Gibson and Sandford*

report such a layer on only two nights within a period of 12 months.

Though we already know some main aspects of the sodium variations in the atmosphere, in day and night time, no exact and well accepted theory exists about the formation and origin of the atmospheric layer of sodium.

An interesting theory presented by *Gadsden* (1970), postulates a meteoric origin for the sodium atoms. Taking into account the deposition of atoms from ablating meteors and subsequent ionization and diffusion, he deduces a model of concentrations where the loss of sodium atoms is mainly due to diffusion into a postulated sink. This model thus involves a continual release of sodium atoms into the atmosphere, rejecting the concept of a constant mixing ratio. The presence of an atom in the atmosphere, is only temporary, being then combined into molecules at lower levels and thus lost from the atmosphere. Though this simplified model presents a sodium distribution similar to the observed one, as noted by *Gibson and Sandford, "it does not seem to predict the observed increase in winter of the concentrations at the peak, or the loss in summer from the topside"*, though the seasonal variation in the diffusion coefficient may contribute to some extent to this effect.

If oxidation of sodium is mainly due to ozone, we will have

$$Na + O_3 \rightarrow NaO + O_2 \qquad (1)$$

and with reduction by O

$$NaO + O \rightarrow Na + O_2 \tag{2}$$

The rates at which NaO and Na are formed may be written as

$$\frac{d[n(NaO)]}{dt} = k_1 \; n(Na) \;\; n(O_3) \tag{3}$$

$$\frac{d[n(Na)]}{dt} = k_2 \; n(NaO) \;\; n(O) \tag{4}$$

where n designates densities and k the rate coefficient.

Equilibrium is achieved when (3) = (4), or when

$$\frac{n(Na)}{n(NaO)} = \frac{k_2}{k_1} \;\; \frac{n(O)}{n(O_3)} \tag{5}$$

The ozone density falls off rapidly with increasing height and thus also the amount of NaO according to reaction (1), and as the degree of dissociation of oxygen becomes larger with altitude, reaction (2) is enhanced. In this way a sharp cutoff is formed below 90 km and the layer formation must be explained by a sodium source which rapidly decreases above this height.

It was stated by *Gibson and Sandford* that *"it appears that reactions other than those with O_3 and O may be important"*. However this conclusion was based on the assumption of a night time increase in O_3, (which would give a consequent decrease in the neutral sodium concentrations, not observed experimentally) and on the assumption of an increase of O_3 during winter (which would lead to a decrease of sodium concentrations during winter, in contrast to the observations). Both assumptions are in contrast with recent calculations by *Shimazaki and Laird*,(1972).

Actually the first assumption above is made on basis of a paper by *Thomas* (1971), and is in fact an extrapolation of an increase of O_3 at lower to higher altitudes. The second was inferred from a paper by *Evans and Llewellyn* (1970) who predict a seasonal variation of a factor of 3 for ozone above 80 km, with maximum in winter based on measurements of the 1.27 μ band of molecular oxygen.

The calculations of *Shimazaki and Laird*, referred above show a rapid jump in ozone density at 90 km, at sunrise/sunset but no variations during the night. For the seasonal variations, they show maximum ozone concentrations during summer and minimum concentrations during winter.

If this new picture of ozone concentrations is true, the almost constant or slightly increasing nighttime sodium abundance might

be easier to understand, though this increase is not yet explained.

Saxena (1969), postulates the Chapman mechanism

$$NaO^* + O \rightarrow Na(^2P) + O_2$$

(* denotes a vibrationally excited state) as responsible for the emission of the sodium lines in the nightglow. He deduces a height profile for the emission rate of the sodium lines that has a maximum at a height around 75 km. As measurements of the sodium layer indicate a maximum around 90 km, he suggested a loss process to reduce the NaO* concentration at altitudes lower than 85 km. The loss reaction proposed was

$$NaO^* + O_3 \rightarrow Na(^2S) + O_2^* + O_2^*$$

and sc a calculated profile was fitted to the observed one. However by just introducing a better model of sodium distribution, such as one measured by the laser radar technique, the calculated nighttime emission rate profile comes to the right height and thus the above loss mechanism no longer seems to be important. The observed increase in the production rate during the night might then be explained by a slight increase in the sodium abundance, as considered possible by *Gibson and Sandford*, if the results of *Shimazaki and Laird* are correct.

Concluding, it is worthwhile saying that no mechanical adjustment of the laser was necessary within these two months.

To begin a set of measurements, the time necessary to set up all the instruments, is at most, half an hour. Only once, within the period, the dye laser's "homemade" flash lamp was changed, with a little more than three thousand shots. It is intended in the near future to change the dye cuvette for a quartz tube. The dye laser is then expected to present a somewhat higher energy. Meanwhile nighttime measurements of the atmospheric sodium layer will continue, in the hope of giving some contribution to solve the problems involved.

APPENDIX I

THE UNITS TRANSFORMATION FROM PULSES TO RAYLEIGHS

The sodium emission is present in the form of two lines at 5896 and 5890 Å. Both reach the PMT passing through a Fabry-Perot interferometer and an interference filter. The sodium signal intensity may thus be written in the form

$$I(Na) = T_{D_1} I_{D_1} \int F(\lambda-\lambda_o)\, d\lambda_o + T_{D_2} I_{D_2} \int F(\lambda-\lambda_o)\, d\lambda_o \quad (1)$$

where T_{D_1} and T_{D_2} are the transmissions of the interference filter at the wavelength of the D_1 and D_2 lines, respectively. I_{D_1} is the intensity in the D_1 line, I_{D_2} in the D_2 line and $F(\lambda-\lambda_o)$ is the Fabry-Perot transmission function. (See Appendix V).

Now let us evaluate the signal intensity for a continuous source which has an intensity $I(\lambda)$ which may be considered constant over the range of interest.

$$I(source) = I(\lambda) \iint T(\lambda)\, F(\lambda-\lambda_o)\, d\lambda\, d\lambda_o \quad (2)$$

where $T(\lambda)$ is the transmission of the interference filter to the intensity

at wavelength λ. This equation may be approximated to

$$I(\text{source}) \doteq I(\lambda) \int T(\lambda)\, d\lambda \int F(\lambda-\lambda_o)\, d\lambda_o$$

because $T(\lambda)$ is almost constant over the Fabry-Perot transmission band.

We thus may relate the two signals, dividing (1) by (2):

$$\frac{I(\text{Na})}{I(\text{source})} = \frac{T_{D_1}\ I_{D_1} + T_{D_2}\ I_{D_2}}{I(\lambda) \int T(\lambda)\, d\lambda} = \frac{A_1}{A_2}$$

where A_1 is the Na signal area and A_2 the source area of the registered pulses. The Na signal is thus

$$T_{D_1}\ I_{D_1} + T_{D_2}\ I_{D_2} = I(\lambda) \int T(\lambda)\, d(\lambda)\, \frac{A_1}{A_2}$$

T_{D_1} and T_{D_2} may be easily measured, the relationship of I_{D_1} and I_{D_2} is also known, the intensity per unit wavelength of the reference source (in our case a radioactive Kr source) $I(\lambda)$ and the area under the interference filter curve are also known quantities so that signal intensities are easily calculated.

For our measurement we have

$$I(\lambda) = 3{,}7 \times 10^{-12} \text{ W/sterad/cm}^2/\text{Å} \quad \text{for Kr source nº 1631}$$

$\int T(\lambda)\, d\lambda = 11$ Å; $T_{D_1} = 0.95$ and $T_{D_2} = 0.9$, relative transmissions.

Putting the units in terms of 10^6 photons per second, square centimeter, sterradian and multiplying by 4π the resultant unit will be the Rayleigh.

Our intensity formula is then

$$I(Na) = 1.67 \times 10^3 \ \frac{A_1}{A_2} \ \text{Rayleigh}$$

For the Kr source nº 1632, $I(\lambda) = 7.8 \times 10^{-12} \text{W/sterad/cm}^2/\text{Å}$ so that

$$I(Na) = 3.52 \times 10^3 \ \frac{A_1}{A_2} \ \text{Rayleigh}$$

APPENDIX II

THE FÜCHTBAUER-LADENBURG FORMULA

This formula relates the integral of the absorption coefficient with the Einstein A coefficient.

Let us consider a parallel beam of light of intensity I_ν, frequency between ν and $\nu + d\nu$, travelling in the positive x direction through a layer of atoms bounded by the planes at x and x + dx. Suppose there are N normal atoms per cubic centimeter of which δN_ν are capable of absorbing the radiation, and N' excited atoms of which $\delta N'_\nu$ are capable of emitting this frequency range. Neglecting spontaneous emission because it takes place in all directions, the decrease in energy of the beam is

$$-d(I_\nu\ \delta\nu) = \delta N_\nu\ dx\ h\nu\ \ B_{12}\ \frac{I_\nu}{4\pi} - \delta N'_\nu\ \ dx\ h\nu\ \ B_{21}\ \frac{I_\nu}{4\pi} \qquad (1)$$

where $I_\nu/4\pi$ is the intensity of the equivalent isotropic radiation for which B_{12} and B_{21} are defined. Rewriting (1) we have

$$-\frac{dI_\nu}{I_\nu\ dx}\ \delta\nu = \frac{h\nu}{4\pi}\ (B_{12}\ \delta N_\nu - B_{21}\ \delta N'_\nu\ )$$

We recognize now that the left hand member is $k_\nu\ \delta\nu$ the

absorption coefficient, defined by

$$I_\nu = I_0 \, e^{-k_\nu \, x}$$

so that we can write

$$k_\nu \, \delta\nu = \frac{h\nu}{4\pi} \, (B_{12} \, \delta N_\nu - B_{21} \, \delta N'_\nu)$$

and integrating now over the whole absorption line, neglecting the slight variation in ν throughout the line,

$$\int k_\nu \, d\nu = \frac{h\nu_0}{4\pi} \, (B_{12} \, N - B_{21} \, N')$$

ν_0 being the center frequency of the line. We now make use of the Einstein's relations:

$$\frac{A_{21}}{B_{12}} = \frac{2h\nu^3}{c^2} \cdot \frac{g_1}{g_2} \qquad \text{(a)}$$

$$\frac{B_{21}}{g_1} = \frac{B_{12}}{g_2} \qquad \text{(b)}$$

where g_1 and g_2 are the multiplicities of the levels and by substitution

we get

$$\int k_\nu \, d\nu = \frac{\lambda_o^2 \, g_2}{8\pi \, g_1} \cdot N A_{21} \left(1 - \frac{g_1}{g_2} \frac{N'}{N}\right)$$

APPENDIX III

THE RAYLEIGH AND RELATED UNITS

Radiant flux density F is the total radiant power crossing a given surface of unit area. The flux unit is then watts/m^2 and is a power density.

Luminous intensity I in a given direction is the flux contained in an infinitesimal cone containing the direction divided by the solid angle of the cone. The units of I are watts/m^2/sterad. The intensity I is also called the integrated intensity (because $I = \int I_\nu \, d\nu$ where I_ν is the specific intensity at frequency ν) or the surface brightness. This photometric quantity is always used in photometry of an extended source.

In the case of atmospheric glows, the source is of the extended kind but we are now interested in the volume emission rate in photons/sec/cm^3.

Let us assume that a given source is emitting F(r) photons/sec/cm^3 in the direction of a photometer at a distance r. The intensity reaching the photometer, from the whole column along the line of sight and of 1 cm^2 cross section is $I = \frac{1}{4\pi} \int F(r)\, dr$ and thus $4\pi I$ is the volume emission rate. Here we assumed that the radiation is emitted isotropically

and that photons once emitted are not subsequently absorbed or scattered in the source. These assumptions are not always justifiable in an accurate analysis and therefore $4\pi I$ represents in general only an *apparent* emission rate.

We define 1 R (one Rayleigh) as an apparent emission rate of one megaphoton/cm^2/sec. If the intensity is measured in units of 10^6 photons/sec/cm^2/sterad, then $4\pi I$ is in Rayleighs.

APPENDIX IV

FABRY PEROT THEORY

Essentially a Fabry Perot interferometer consists of two parallel glass plates. The inner surfaces are coated with partially transparent films of high reflectivity and are plane to a high degree of accuracy. If a ray of light is incident on the surfaces, through an angle θ, multiple scattering will occur between the surfaces and at each point of incidence on the second surface, a set of parallel rays will be transmitted, (see figure 28). This transmission at wavelength λ will be a maximum if the path difference between successive rays in an integral number of wavelength, i.e., if

$$2\, d \cos\theta = n\, \lambda$$

where d is the separation between the flat surfaces (which actually are high quality mirrors) and n is an integer denoting the order of interference. Thus an etalon tilted through an angle works like a filter.

The transmission peak of the Fabry Perot is not single but repeats at regular intervals of wavelength. The wavelength difference between two successive transmission peaks is called the free spectral

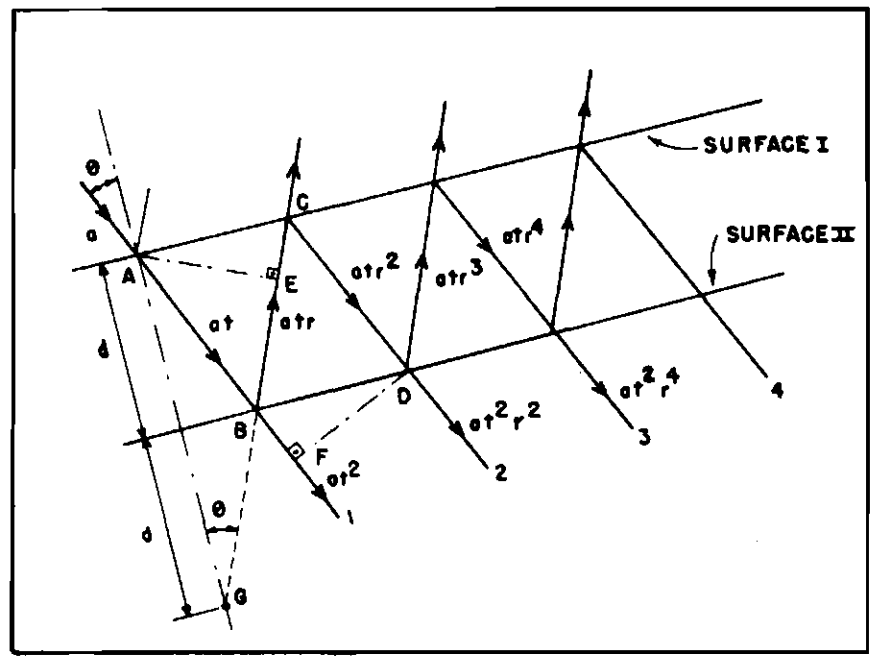

Fig. 28 - Multiple reflections

range $\Delta\lambda$ and is given by

$$\Delta\lambda = \frac{\lambda^2}{2d}$$

where λ is the mean wavelength of the radiation and d is the mirror separation.

When the transmitted rays are brought together by means of a lens, interference fringes in form of rings are formed and these may be used for wavelength comparisons. The etalon surfaces are generally highly reflective for fringe observation because the sharpness of the fringes is better with higher reflection coefficient. The relation between the free spectral range and the bandwidth of the transmission peak is the finesse of the instrument. It is given essentially by

$$F = \frac{\pi R^{1/2}}{1 - R}$$

but also depends on diffraction, plate parallelism and plate figure limitations.

Surface I and II (figure 28) have reflection coefficients for amplitude equal to r, and transmission coefficients for amplitude equal to t. Absorption is neglected.

The optical path difference between successive transmitted rays 1, 2, 3, ... is

$$\Delta = m\,(BC + CD) - BF$$

where m is the refractive index of the medium between the plates (air), taken equal to unity. From figure 28 we see that (BC + CD) is equal to GC and that BF is equal to EC so that

$$\Delta = GC - EC = GE = 2d\cos\theta$$

Thus the phase difference between successive rays is

$$\delta = \frac{2\pi}{\lambda}\ \Delta = \frac{2\pi}{\lambda}\ 2d\cos\theta$$

and the sum of rays 1, 2, 3, ... will be

$$Ae^{i\psi} = at^2 + at^2 r^2 e^{i\delta} + at^2 r^4 e^{i2\delta} + \ldots$$

$$= a(1 - r^2)\,(1 + r^2 e^{i\delta} + r^4 e^{i2\delta} + \ldots)$$

$$= \frac{a(1 - r^2)}{1 - r^2 e^{i\delta}}$$

where we substituted t^2 by $1 - r^2$ and the infinite geometric series by its sum.

Multiplication by the complex conjugate gives us the intensity

$$I_T \propto \frac{a\,(1 - r^2)\; a\,(1 - r^2)}{(1 - r^2\, e^{i\delta})(1 - r^2\, e^{-i\delta})}$$

$$= \frac{a^2\,(1 - r^2)^2}{1 - r^2\,(e^{i\delta} + e^{-i\delta}) + r^4}$$

and since $a^2 \propto I_0$, the intensity of the incident beam, $(e^{i\delta} + e^{-i\delta})/2 = \cos\delta$, we have

$$\frac{I_T}{I_0} = \frac{(1 - r^2)^2}{1 - 2r^2\cos\delta + r^4}$$

$$= \frac{1}{1 + \dfrac{4r^2}{(1 - r^2)^2}\,\sin^2\dfrac{\delta}{2}}$$

or if we write $r^2 = R$, the reflection coefficient for power,

$$\frac{I_T}{I_o} = \frac{1}{1 + \frac{4R}{(1 - R)^2} \sin^2 \frac{\delta}{2}}$$

which is the Fabry Perot transmission function.

APPENDIX V

LIST AND COMMENTS ON LASNA, TWI AND KIRAN

1.- LASNA stands for Laser Radar measurements of atmospheric sodium. It calculates the density at height h and the corresponding standard deviation. For each set of 100 laser shots a density profile is plotted and for the number L of profiles a mean is deduced.

The program data are:

a) the number of profiles to be calculated (L); and
b) the measured count values from channel 52 to channel 31 and the count from channel 10.

The first 13 points are the profile data values. From 14 to 31 are the noise channels and channel 10 is the reference Rayleigh signal at 20 km.

The following data values are calculated and written separately: *DENS*, the density values in units of 10^9 m^{-3} at heights from 104 to 80 km; *DENS SUP*, i.e., the density values plus the standard deviation; *TRUE*, the true sodium count (or the count minus the noise) per shot; *NOISE*, the mean noise for the profile, per shot; *RAY 20*, the Rayleigh count at 20 km per shot; and *K 20 km*, the constant K of the equipment.

2.- TWI stands for Twilight. It only plots the measured twilight spectrum and calculates the area under the curve. The total number of profiles must be given and the 56 data values.

3.- KIRAN stands for the calculation of the depression angle of the sun E. (Also sometimes called elevation angle). The calculation is done for each twilight run, furnishing the sun's depression angle and the height of the effective shadow at a certain time, according to the equations of Chapter II.

Six data values must be furnished to the data card:

1) the initial time (sunset time or sunrise minus 50 min) hours;
2) the initial time, minutes;
3) the Greenwich hour angle θ, for midnight, degrees and
4) minutes;
5) the sun's declination angle, degrees and
6) minutes.

These data values are found in the Nautical Almanac.

```
IDENT SODIO
FILE  6=LASER,UNIT=PRINTER
FILE  5=LAS
C
C     PERFIS DE SODIO MEDIDOS COM O RADAR= LASNA
C
C     ALIMENTAR COM O VALOR DO NUMERO DE PERFIS,(L), E SHOT NUMBER (SN)
C
      DIMENSION RO(20),ROI(20),ROS(20),CA(12,28),CNA(12),H(20),F(20)
      DATA FS,SN,N3,N4/172.4,100.,14,22/
  200 L=3
      M=L+1
      DO 41 J=1,L
   41 READ(5,10) (CA(J,I),I=1,23)
      DO 54 I=1,23
      CA(L+1,I)=0.
      DO 55 J=1,L
   55 CA(M,I)=CA(M,I)+CA(J,I)/FLOAT(L)
   54 CONTINUE
      DO 56 J=1,M
      SUM=0.
      DO 20 I=N3,N4
   20 SUM=SUM+CA(J,I)
      CNA(J)=SUM/(9.*SN)
   56 CONTINUE
      CALL PLOTS
      CALL PLOT(0.,-11.,-3)
      CALL PLOT(0.,.25,-3)
      DO 99 J=1,M
      HA=104.*10.**3
      FAR=CA(J,23)/(SN)
      FTI=FAR*EXP(FAR/FS)
      DO 1 K=1,30
      FT=(FS*FAR*EXP(FT1/FS)-FT1**2)/(FS-FT1)
      IF(ABS(FT-FT1).LT.1.E-5)GO TO 2
    1 FT1=FT
    2 C20=FT
      WRITE(6,100)
      SUM2=0.
      DO25 I=1,13
      FA=CA(J,I)/(SN)
      FTI=FA*EXP(FA/FS)
      DO 30 IK=1,30
      FT=(FS*FA*EXP(FTI/FS)-FTI**2)/(FS-FTI)
      IF(ABS(FT-FTI).LT.1.E-5)GO TO 35
   30 FTI=FT
   35 CONTINUE
      IF(J-L)31,31,32
   31 DF=SQRT(FT/(SN))
      GO TO 33
   32 DF=SQRT(FT/(SN*FLOAT(L)))
   33 F(I)=FT-CNA(J)
      RK20=5.*10.**24*C20
      RO(I)=F(I)*HA**2*10.**16*3.1416/RK20
      IF(RO(I).LT.0.0) RO(I)=0.
      SUM2=SUM2+RO(I)
      DRO=DF*HA**2*10.**16*3.1416/RK20
      ROS(I)=RO(I)+DRO
      ROI(I)=RO(I)-DRO
      IF(ROI(I).LT.0.0) ROI(I)=0.
      H(I)=HA/(10.**3)
```

```
      WRITE(6,40) H(I),RO(I),ROS(I),F(I),CNA(J),C20,RK20
      HA=HA*2.*10.**3
   25 CONTINUE
      AREA=(2.*SUM2-RO(1)-RO(13))/10.
      WRITE(6,400)
      WRITE(6,300) AREA
      G=1./2.54
      CALL FACTOR(G)
      CALL AXIS(0.,0.,11HALTURA (KM),-11,8.,0.,112.,-4.)
      CALL AXIS(0.,0.,15HDENSIDADE (M-3),15,25.,90.,0.,0.4)
      H(14)=112.
      H(15)=-4.
      RO(14)=0.
      RO(15)=0.4
      CALL LINE(H,RO,13,1,0,0)
      DO 70 N=1,13
      X=H(N)
      X=(112.-X)/4.
      Y=ROS(N)
      Y=Y*2.5
      Z=ROT(N)
      Z=Z*2.5
      CALL PLOT(X,Y,3)
      CALL PLOT(X,Z,2)
   70 CONTINUE
      CALL PLOT(+12.,0.,-3)
   99 CONTINUE
      CALL PLOT(1.,1.,999)
   10 FORMAT(8F10.0)
  100 FORMAT(//6X,3HALT,11X,4HDENS,3X,8HDENS SUP,5X,4HTRUE
     2,5X,5HNOISE,5X,5HRAY20,8X,7HK 20 KM)
   40 FORMAT(F10.1,4X,F10.2,4X,4(F6.2,4X),2X,E10.2)
  300 FORMAT(50X,F5.2)
  400 FORMAT(/48X,9HABUNDANCE)
      STOP
      END

06/30/72     9245 AM    ASR#4.5     63072     COMPILER
  0 MIN 34 SEC FOR COMPILATION PASS
   98 CARDS AT 171 CARDS PER MINUTE
  6696 DIGITS DATA.  7210 DIGITS CODE.
```

```
IDENT SODIO
FILE  6=LASER,UNIT=PRINTER
FILE  5=RUN
C     PERFIL DA INTENSIDADE VS CANAL - TWI
C     L E O NUMERO DE PERFIS A FAZER
      DIMENSION Y(60), X(60)
      CALL PLOTS
      CALL PLOT(0.,-10.5,-3)
      CALL PLOT(0.,.5,-3)
      F=1./2.54
      CALL FACTOR(F)
      READ(5,1) L
    1 FORMAT(I10)
      DO 10 J=1,L
      READ(5,20) (Y(I),I=1,56)
      SUM=0.
      DO 30 I=1,56
      SUM=SUM+Y(I)
   30 CONTINUE
      AREA=(2.*SUM-Y(1)-Y(56))/2.
      WRITE(6,50) AREA
      X(1)=1.
      DO 40 K=1,55
      X(K+1)=X(K)+1.
   40 CONTINUE
      CALL PLOT(33.,0.,-3)
      CALL AXIS(0.,0.,5HCANAL,-5,11.,0.,0.,5.)
      CALL AXIS(0.,0.,20HINTENSIDADE RELATIVA,+20,20.,90.,0.,100.)
      CALL SYMBOL(14.,7.,.2,22HAREA=        ,D2/D1=    ,0.,22)
      Y(57)=0.
      Y(58)=100.
      X(57)=0.
      X(58)=5.
      CALL LINE(X,Y,56,1,0,0)
   10 CONTINUE
      CALL PLOT(1.,1.,999)
   20 FORMAT(8F10.0)
   50 FORMAT(F8.1)
      STOP
      END

04/26/72     2218 PM    ASR#4.5     42672     COMPILER
  0 MIN 16 SEC FOR COMPILATION PASS
   41 CARDS AT 154 CARDS PER MINUTE
  2070 DIGITS DATA.  1744 DIGITS CODE.
```

```
IDENT SUDID
FILE  6=LASER,UNIT=PRINTER
FILE  5=DYE
C
C      THE SUNS ELEVATION ANGLE E DURING TWILIGHT - KIRAN
C      L E O NUMERO DE CARTOES COM DADOS ATE 16
C      ALIMENTAR COM O VALOR DE L E OS DADOS COMO EM READ
C
       DIMENSION G1(20),G2(20),T1(20),T2(20),D1(20),D2(20),D(20)
       DIMENSION GHA(70),GMT(20,70),E(70),ALT(70),SE(70),CE(70),TET(20)
       L=6
       DO 20 N=1,L
       READ(5,80) G1(N),G2(N),T1(N),T2(N),D1(N),D2(N)
       WRITE(6,90)
       WRITE(6,100) G1(N),G2(N),T1(N),T2(N),D1(N),D2(N)
       GMT(N,1)=G1(N)+G2(N)/60.
       TET(N)=(T1(N)+T2(N)/60.)*3.1416/180.
       D(N)=(D1(N)+D2(N)/60.)*3.1416/180.
       DO 10 I=1,60
       GHA(1)=(GMT(N,I)*15.*3.1416/180.)+TET(N)
       GMT(N,I+1)=GMT(N,1)+1./60.
   10  CONTINUE
       WRITE(6,40)
       WRITE(6,50)
       DO 30 I=1,60
       A=D(N)
       SE(I)=COS(GHA(I)-45.50*3.1416/180.)*.9191*COS(D(N))-.3942*SIN(A)
       CE(I)=SQRT(1.-SE(I)*SE(I))
       E(I)=ATAN(SE(I)/CE(I))
       E(I)=E(I)*180./3.1416
       ALT(I)=(1./CE(I))*6401.-6371.
       WRITE(6,70) GMT(N,I), E(I), ALT(I)
   30  CONTINUE
   20  CONTINUE
   80  FORMAT(6F10.0)
   90  FORMAT(//2X,3HGMT HORA,6X,3HMIN,4X,9HTET GRAUS,4X,3HMIN,4X,9HDEC G
      2RAUS,3X,3HMIN)
  100  FORMAT(/4X,6(F6.1,4X))
   40  FORMAT(/15X,31HDADOS DO DIA     MES     ANO      )
   50  FORMAT(//5X,3HGMT,9X,1HE,10X,6HALT KM)
   70  FORMAT(4X,F5.2,5X,F6.1,6X,F6.1)
       STOP
       END

05/09/72      3:26 PM    ASR#4.5     50972     COMPILER
  0 MIN 19 SEC FOR COMPILATION PASS
   44 CARDS AT 134 CARDS PER MINUTE
 23572 DIGITS DATA.  4772 DIGITS CODE.
```

ACKNOWLEDGEMENTS

I acknowledge the interest of the examination committee in the persons of Dr. Fernando de Mendonça, Dr. Barclay Robert Clemesha, Dr. Kalvala Ramanuja Rao, and Dr. Luiz Gylvan Meira Filho. Special thanks are directed to Dr. B.R. Clemesha, teacher and adviser, under whose guidance this work was done. Useful discussions held with Dr. Luiz Gylvan Meira Filho and the assistance of INPE's workshop are acknowledged. My thanks are also due to my wife for her great assistance and typing.

REFERENCES

1.- BAIN, W.C., and M.C.W. Sandford, *J. Atmosph. Terr. Phys*, 28, 543, 1966.

2.- BLAMONT, J.E., and T.M. Donahue, *J. Geophys. Res.*,66, 1407, 1961.

3.- BLAMONT, J.E., and T.M. Donahue, *J. Geophys. Res.*, 69, 4093, 1964.

4.- BOWMAN, M.R., A.J. Gibson and M.C.W. Sandford, *Nature*, 221, 456, 1969.

5.- BRACEWELL, R.N., *J. Opt. Soc. Amer.*, 45, 873, 1955.

6.- BRANDT, J.C., and J.W. Chamberlain, *J. Atmosph. Terr. Phys.*, 13, 90, 1958.

7.- CHAMBERLAIN, J.W., *Physics of the Aurora and Airglow*, Acad. Press, New York, 1961.

8.- CLEMESHA, B.R., G.S. Kent and R.W.H. Whright, *Nature*, 210, 184, 1966.

9.- CLEMESHA, B.R. and V.W.J.H. Kirchhoff, *INPE Internal Report*, 3, May 1972.

10.- DONAHUE, T.M., *Int. Dict. Geophys.* Pergamon Press, New York, 1966.

11.- DONAHUE, T.M., *J. Geophys. Res.*, 61, 663, 1956.

12.- DONAHUE, T.M. and R.R. Meier, *J. Geophys. Res.*, 72 (11), 2803, 1967.

13.- EVANS, W.F.J. and E.J. Llewellyn, *Annls. Geophys.*, 26, 167, 1970.

14.- FIOCCO, G. and G. Grams, *J. Atmos. Sci.*, 21, 323, 1964.

15.- GADSDEN, M., *J. Atmosph. Terr. Phys.*, 30, 151, 1968.

16.- GADSDEN, M., *Annls. Geophys.*, 20, 261, 1964.

17.- GADSDEN, M., *Annls. Geophys.*, 20, 383, 1964.

18.- GADSDEN, M., *Annls. Geophys.*, 26, 141, 1970.

19.- GIBSON, A.J., *J. Sci. Inst.*, 2, 802, 1969.

20.- GIBSON, A.J., and M.C.W. Sandford, *J. Atmosph. Terr. Phys.*, 28, 543, 1971.

21.- HUNTEN, D.M., *J. Atmosph. Terr. Phys.*, 24, 333, 1962.

22.- HUNTEN, D.M., *J. Atmosph. Terr. Phys.*, 17, 295, 1960.

23.- HUNTEN, D.M., *Science*, 145, 26, 1964.

24.- HUNTEN, D.M., A.V. Jones, C.D. Ellyett, and E.C. MacLauchlan, *J. Atmosph. Terr. Phys.*, 26, 67, 1964.

25.- HUNTEN, D.M. and L. Wallace, *J. Geophys. Res.*, 72, (1), 69, 1967.

26.- HUNTEN, D.M., *Space Sci. Rev.*, 6, 493, 1967.

27.- JONES, A.V., *Planet. Space Sci.*, 10, 117, 1963.

28.- JUNGE, C.E., O. Oldenberg, and J.T. Wasson, *J. Geophys. Res.*, 67, (3), 1027, 1962.

29.- KIRCHHOFF, V.W.J.H., *ITA Engenharia,* 3, (1), 1972.

30.- LEVENS, A.S., *Graphical Methods in Research,* John Wiley & Sons, Inc., 1965.

31.- MOTISUKE, P., *LAFE-143,* INPE, 1970.

32.- RODRIGUES, S.N., *LAFE-136,* INPE, 1970.

33.- SANDFORD, M.C.W., and A.J. Gibson, *J. Atmosph. Terr. Phys.,* 32, 1423, 1970.

34.- SAXENA, P.P., *Annls. Geophys.,* 26, 505, 1970.

35.- SAXENA, P.P., *Annls. Geophys.,* 25, 847, 1969.

36.- SHIMAZAKI, T., and A.R. Laird, *Radio Science,* Jan. 1972.

37.- SOROKIN, P., *Scient. Amer.,* Feb. 1969.

38.- STONG, C.L., *Scient. Amer.,* Jan. 1970.

39.- THOMAS, L., *J. Atmosph. Terr. Phys.,* 33, 157, 1971.

40.- TINSLEY, B.A. and A.V. Jones, *J. Atmosph. Terr. Phys.,* 24, 345, 1962.

41.- WEBER, M.J. and M. Bass, *IEEE, J. Quant. Elec.,* Q.E 5, (4), 1969.